

# Recent Advances in Solar-Driven Carbon Dioxide Conversion: Expectations versus Reality

Jie He and Csaba Janáky\*

Cite This: *ACS Energy Lett.* 2020, 5, 1996–2014

Read Online

ACCESS |



Metrics &amp; More

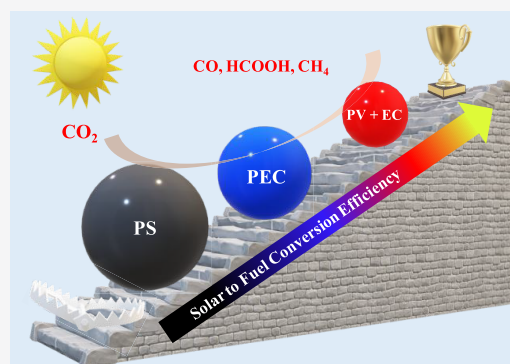


Article Recommendations



Supporting Information

**ABSTRACT:** Solar-driven carbon dioxide ( $\text{CO}_2$ ) conversion to fuels and high-value chemicals can contribute to the better utilization of renewable energy sources. Photosynthetic (PS), photocatalytic (PC), photoelectrochemical (PEC), and photovoltaic plus electrochemical (PV+EC) approaches are intensively studied strategies. We aimed to compare the performance of these approaches using unified metrics and to highlight representative studies with outstanding performance in a given aspect. Most importantly, a statistical analysis was carried out to compare the differences in activity, selectivity, and durability of the various approaches, and the underlying causes are discussed in detail. Several interesting trends were found: (i) Only the minority of the studies present comprehensive metrics. (ii) The  $\text{CO}_2$  reduction products and their relative amount vary across the different approaches. (iii) Only the PV+EC approach is likely to lead to industrial technologies in the midterm future. Last, a brief perspective on new directions is given to stimulate discussion and future research activity.



Carbon dioxide ( $\text{CO}_2$ ) is one of the main greenhouse gases contributing to global climate change.<sup>1</sup> According to the National Oceanic and Atmospheric Administration (United States), the global mean  $\text{CO}_2$  level reached 410 ppm in 2019.<sup>2</sup> To cope with climate challenge, more than 170 nations signed the Paris agreement in 2016, committing to fight climate change by cutting  $\text{CO}_2$  emissions.<sup>3</sup> Such a political ambition requires a paradigm shift, supported by technological breakthroughs. One such change is to consider  $\text{CO}_2$  as an abundant carbon source, instead of a pollutant. The turn-waste-into-wealth strategy will certainly play a key role in the green transformation of the chemical industry.<sup>4–6</sup> There are numerous routes to convert  $\text{CO}_2$  to fuels and other chemicals. From the overall energy payback perspective, however, the most promising methods are those employing renewable energy. In this Focus Review, we focus on solar energy, which is regarded as a clean, abundant, and free renewable energy source. About 10% of the solar energy received on 0.3% of the Earth's surface would be enough to fulfill the expected energy needs in 2050.<sup>7</sup> Therefore, the combination of solar energy utilization and  $\text{CO}_2$  resources can be expected to produce fuels as well as value-added chemicals. Moreover, beyond their cost-effectiveness, such processes are environmentally friendly and carbon-neutral.<sup>8</sup>

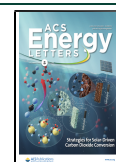
The conversion of  $\text{CO}_2$  can lead to several different chemical/fuel products depending on the materials and/or methods employed, including carbon monoxide ( $\text{CO}$ ), formic acid ( $\text{HCOOH}$ ), methane ( $\text{CH}_4$ ), methanol ( $\text{CH}_3\text{OH}$ ), ethylene ( $\text{C}_2\text{H}_4$ ), ethane ( $\text{C}_2\text{H}_6$ ), propane ( $\text{C}_3\text{H}_8$ ), ethanol ( $\text{CH}_3\text{CH}_2\text{OH}$ ), acetic acid ( $\text{CH}_3\text{COOH}$ ), acetone, *n*-propanol, acetaldehyde, allyl alcohol, dimethyl ether, glycolaldehyde, hydroxyacetone, ethylene glycol, propionaldehyde, and glycerol.<sup>9</sup> Although the carbon content of these products, at the current production level, accounts for only a fraction of the emitted  $\text{CO}_2$ ,<sup>10</sup> the concept of solar-driven  $\text{CO}_2$  can be extended to fuel production in the future (especially for aviation where high energy density is inevitable), which accounts for a much larger carbon footprint.<sup>5</sup>

Since the discovery of photoinduced reduction of  $\text{CO}_2$  on semiconductors,<sup>11</sup> enormous research efforts have been devoted to the solar-driven conversion of  $\text{CO}_2$ , and the field has witnessed a renaissance in the past few years.<sup>7,8,12–30</sup> We

Received: March 23, 2020

Accepted: May 15, 2020

Published: May 15, 2020



collected the number of papers published between 2014 and 2019 from the Web of Science database. There is a 3-fold increase in the number of published papers since 2014 (Figure 1), indicating the continuously growing research interest.

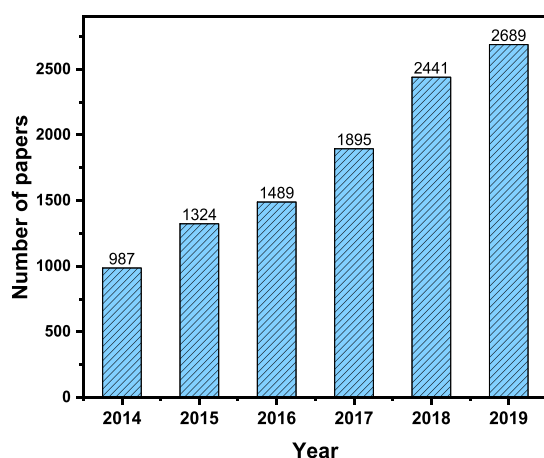


**Figure 1.** Number of papers published in the years of 2014–2019. Data collected from Web of Science Core Collection on 2020-03-06; topic: (photo\* or solar) and (CO<sub>2</sub> or carbon dioxide) and (conversion or reduction).

In fact, this trend also follows the policy orientation of national governments and international funding agencies. Energy-X<sup>5</sup> and Sunrise<sup>31</sup> started as independent projects, supported by the European Union's Horizon 2020 research and innovation program, focusing on the science and technology enabling efficient conversion of solar energy into chemicals. They are now merged into the "SUN-ERGY" program, to join forces under the umbrella of Horizon Europe, also in line with the Solar-Driven Chemistry Initiative of the European Chemical Society (EuChemS).<sup>32</sup> In the United States, the Joint Center for Artificial Photosynthesis (JCAP) was established in 2010, aiming to find new and effective ways to produce fuels using only sunlight, water, and CO<sub>2</sub>. It is the largest research program in the United States dedicated to the advancement of solar-fuels generation science and technology.<sup>33</sup> Other national programs are being implemented around the world, focusing on both fundamental science and technology development.

Considering the current momentum of the field and the expectations of the funders (ultimately the society), there is a need to scrutinize the recent scientific and technological

achievements. This exercise can shed light on what is competitive (and what remains in the land of promise) and also help to identify the most promising directions for newcomers to the field. There are a lot of books, book chapters, and review articles focusing on solar-driven CO<sub>2</sub> reduction topics, and the aim of this Focus Review is not to repeat such information. In contrast, our approach is to compare precedent results, based on metrics that can be employed as overarching benchmarks through the various solar-driven CO<sub>2</sub> conversion technologies. In addition, we highlight a few studies in which outstanding performances were achieved for a given metric.

**Different Solar-Driven CO<sub>2</sub> Conversion Approaches.** Solar-driven CO<sub>2</sub> conversion methods can be categorized into biophotosynthetic, photothermal, microbial-photoelectrochemical, photosynthetic (PS), photocatalytic (PC), photoelectrochemical (PEC), photovoltaic plus electrochemical (PV+EC), etc. The classification and definitions of solar-driven CO<sub>2</sub> conversion approaches involved in this review article are summarized in Table 1. The schematic illustrations of these systems together with the operational principles are also shown in Figure 2. Biophotosynthetic CO<sub>2</sub> conversion mimics natural photosynthesis and therefore usually involves redox enzyme molecules as photocatalysts or artificial microbes for photosynthesis.<sup>34–40</sup> The photothermal CO<sub>2</sub> conversion approach uses high-temperature solar reactors, typically concentrated solar radiation, to split CO<sub>2</sub>, potentially offering high product formation rate.<sup>41–50</sup> Microbial PEC CO<sub>2</sub> conversion combines the advantages of semiconductor nanodevices and the high-selectivity biocatalysts, directly converting CO<sub>2</sub> into fuels or chemicals.<sup>51–53</sup> Among the above-mentioned pathways, PS, PC, PEC, and PV+EC approaches are more commonly studied, because they are mostly carried out under relatively mild conditions, such as low temperature and ambient pressure. These strategies will be discussed in detail later; here, only a brief overview is provided.

Our approach was to compare precedent results, based on metrics which can be employed as overarching benchmarks through the various solar-driven CO<sub>2</sub> conversion technologies.

**Table 1.** Classifications and Definitions of Solar-Driven CO<sub>2</sub> Conversion Approaches

category	definition
Biophotosynthetic	An approach that mimics natural photosynthesis, which usually involves redox enzyme molecules as photocatalysts or artificial microbes for photosynthesis
Photothermal	An approach that uses high-temperature solar reactors, typically employing concentrated solar radiation, to split CO <sub>2</sub> , potentially utilizing the entire solar spectrum and offering high product formation rate
Microbial-photoelectrochemical	Combines the advantages of semiconductor photoelectrodes and the high-selectivity microbe-based biocatalysts, directly converting CO <sub>2</sub> into fuels or chemicals
Photosynthetic and photocatalytic (PS/PC)	Two sister approaches using particulate or molecular photocatalysts, either in solution or immobilized on a surface. This category includes both PC ( $\Delta G < 0$ ) and PS ( $\Delta G > 0$ ) processes, depending on the oxidation half reaction. Because of many similarities, they are discussed together herein, but in the light-to-fuel efficiency comparison (Figure 9b), only PS processes were selected to ensure fair comparison.
Photoelectrochemical (PEC)	Either one or both electrodes of the electrochemical cell is/are semiconductor photoelectrode(s). Photogenerated charge carriers drive either one or both half reactions. We included studies using the "buried junction" concept here, where a solar cell is covered by one or more catalyst(s) (and possibly a protecting layer) and this whole assembly acts as a photoelectrode.
Photovoltaic plus electrochemical (PV+EC)	The combination of PV cells with CO <sub>2</sub> electrolysis in one device. This approach decouples the light-harvesting and the electrochemical conversion steps.

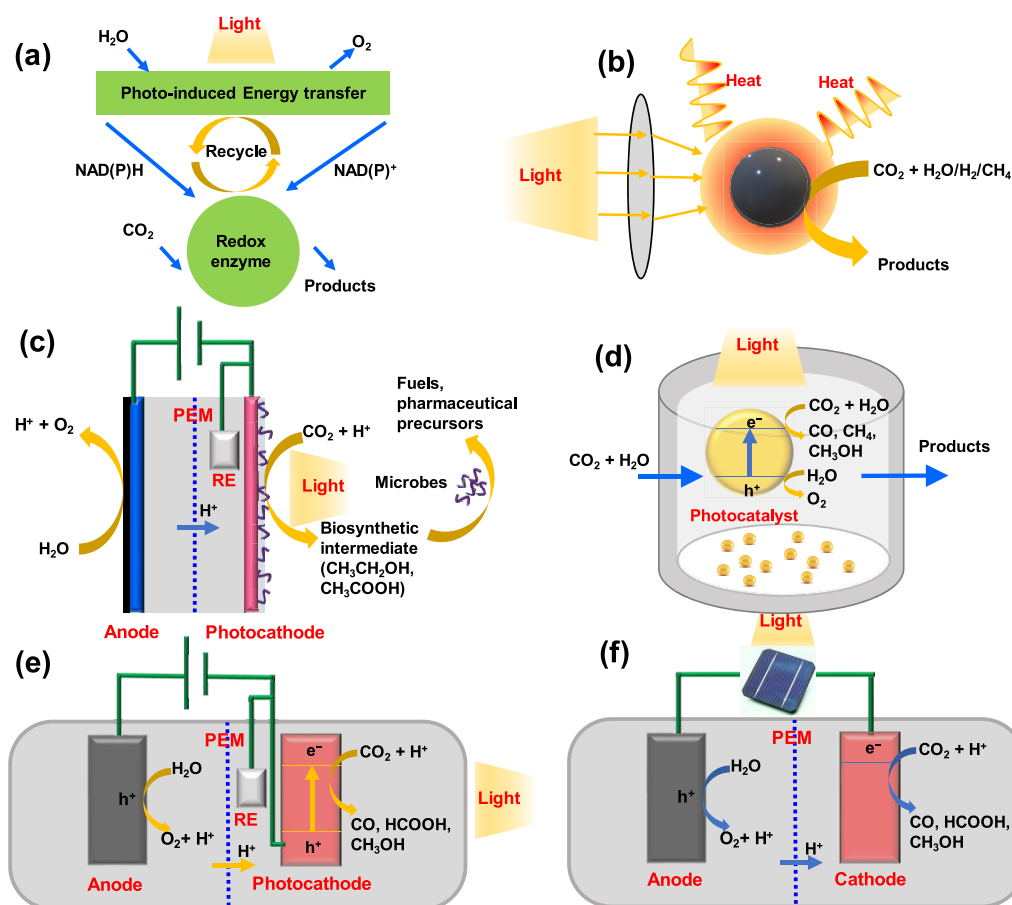


**Figure 2.** Schematic illustration of (a) biophotosynthetic, (b) photothermal, (c) microbial-photoelectrochemical, (d) photosynthetic and photocatalytic (PS/PC), (e) photoelectrochemical (PEC), and (f) photovoltaic plus electrochemical (PV+EC) approaches for CO<sub>2</sub> conversion.

There are many studies using sunlight to convert CO<sub>2</sub> over molecular or semiconductor photocatalysts, the so-called photosynthetic (PS) and photocatalytic (PC) processes. Notably, relevant chemical literature often does not differentiate between these two, although these reactions differ in their thermodynamics. PC processes are thermodynamically downhill ( $\Delta G < 0$ ) and are purely accelerated by the catalyst, whereas PS processes are thermodynamically unfavorable ( $\Delta G > 0$ ) and require photochemical energy input to occur. When CO<sub>2</sub> reduction is paired with the oxygen evolution reaction, it is an uphill reaction ( $\Delta G > 0$ ); thus, it should be defined as a PS process.<sup>54,55</sup> In contrast, if it is coupled with an anode process where a hole-scavenger is present, it can indeed be a PC process. This distinction is important, because there are different descriptors defining the performance in the two scenarios.<sup>54</sup> While similar solar light harvesting, charge separation, and transportation processes occur, the surface reactions and recombination are very different in the two cases.<sup>19,55,56</sup> Because of the many similarities, they are discussed together herein, except for the light-to-fuel conversion efficiency comparison.

Although hundreds of photocatalysts are reported yearly to demonstrate their effectiveness, many of these studies suffer from fundamental problems. Most of these studies focus only on the reduction part of the process such as the transformation of CO<sub>2</sub> to CO, CH<sub>4</sub>, and HCOOH, but the coupled oxidation process (the other half of the story) is seldom discussed in

detail. It has been a common practice to include sacrificial electron donors such as triethanolamine in a PC reaction to overcome both thermodynamic and kinetic limitations of the oxidation process. This practice, however, requires careful attention: (1) the process should be defined as PC rather than PS (see above); (2) the reported light-to-fuel conversion efficiencies might be inaccurate; (3) the oxidation of sacrificial donors may contribute to the products that are being considered as CO<sub>2</sub>-reduction products. There are at least two possible ways how a sacrificial donor can “contribute” to assumed CO<sub>2</sub>-reduction products: either the oxidation of the sacrificial electron donors directly produces C<sub>1</sub> products, or the radical intermediates produced in the oxidation process have reductive abilities, which help to convert CO<sub>2</sub>. Therefore, if applied, it is very important to evaluate the fate of these sacrificial donors and their contributions to the overall yield of the products in the PC CO<sub>2</sub> reduction reactions.<sup>57,58</sup>

Compared with the particle suspension-based PS and PC process, the photoelectrode-based PEC reduction of CO<sub>2</sub> can integrate the advantages of photosynthesis and electrocatalysis.<sup>59</sup> Based on which electrode acts as the light absorber, three different PEC configurations can be envisioned: photocathode–dark anode (shown in Figure 2e as an example), photoanode–dark cathode, and photocathode–photoanode. The fact that each photoelectrode can consist of multiple absorber layers to better cover the solar spectrum complicates the picture further. A sophisticated variant is the

Table 2. Summarized Performance Metrics for PS/PC, PEC, and PV+EC Systems

	PS/PC	PEC	PV+EC
Performance metrics	Formation rate Conversion Turnover number (TON) Selectivity Quantum efficiency (QE) Durability	Formation rate (current density) Potential/voltage Selectivity (Faradic efficiency, FE) Solar-to-fuel conversion efficiency (SFE) Incident photon-to-current conversion efficiency (IPCE) Absorbed photon-to-current conversion efficiency (APCE) Durability	Formation rate (current density) Potential/voltage Selectivity (Faradic efficiency, FE) Solar-to-fuel conversion efficiency (SFE) Durability

Table 3. Selected Studies on PS/PC CO<sub>2</sub> Conversion

PS								
catalyst	illumination conditions	reactant/ solution	products	QE (%)	selectivity (%)	formation rate normalized (mmol e <sup>-</sup> g <sub>cat</sub> <sup>-1</sup> h <sup>-1</sup> )	maximum test time (h)	ref.
Surface S and Br modified CoO/Co <sub>3</sub> O <sub>4</sub>	300 W Xe lamp, <sup>2</sup> 500 mW cm <sup>-2</sup>	H <sub>2</sub> O	CH <sub>4</sub>	2.3 at 405 nm	98	~80	9	99
CuIn <sub>5</sub> S <sub>8</sub> single-unit-cell layers	AM 1.5G filter, λ ≥ 400 nm, ~50 mW cm <sup>-2</sup>	H <sub>2</sub> O	CH <sub>4</sub>	0.79	100	0.0696	120	100
(Ag@Cr)/Ga <sub>2</sub> O <sub>3</sub>	400 W high-pressure mercury lamp with a quartz filter	H <sub>2</sub> O	CO		85.2	2.1	5	101
PC								
catalyst	illumination conditions	reactant/solution	products	QE (%)	selectivity (%)	formation rate normalized (mmol e <sup>-</sup> g <sub>cat</sub> <sup>-1</sup> h <sup>-1</sup> ) or TON	maximum test time (h)	ref.
Co–Co <sub>2</sub> P@ NPC	200 W white LED lamp	TEOA/H <sub>2</sub> O/MeCN, [Ru(bpy) <sub>3</sub> ]Cl <sub>2</sub> ·6H <sub>2</sub> O	CO		79.1	~70	18	102
RuP/C <sub>3</sub> N <sub>4</sub>	400 W Hg lamp, λ > 400 nm	DMA/TEOA	HCOOH	5.7 at 400 nm		TON > 1000		103
Iridium(III) complexes	Blue LED light, 0.43 mW cm <sup>-2</sup>	TEOA/MeCN	CO	10		TON > 265	10 days	104

“buried junction” concept, where a solar cell is covered by one or more catalyst(s) (and possibly a protecting layer) and this whole assembly acts as a photoelectrode.<sup>60–63</sup>

Development in photovoltaic (PV) technologies over the past 5–10 years is eye-catching, with the record of light-to-electrical power conversion efficiency (PCE, which is the ratio between the incident solar photon energy and the electrical energy output) being continuously renewed.<sup>64</sup> For example, the silicon-based single-junction PV cell could achieve the PCE of 26.7%; the III–V single-junction cells, such as GaAs, reached the PCE of as high as 29.1%, while the burgeoning perovskite-based cells could also achieve 21.6%. The multi-junction cells, such as AlGaInP/AlGaAs/GaAs/GaInAs further increased the PCE to 47.1%.<sup>65,66</sup> What is equally important, with the rapid growth of the PV industry, the price of the Si-based PV cells has declined sharply.<sup>67</sup> Therefore, these low-cost and reliable silicon-based PV modules are widely available. PV cells can be combined with an electrolyzer, thus decoupling the light-harvesting (current generation) and the electrochemical conversion steps (PV+EC system). For the PV+EC systems discussed in this Focus Review, we excluded those studies where a solar cell covered by a catalyst acts as a photoelectrode for one half reaction (those are discussed in the PEC field). Only those scenarios are considered where the PV panel is the sole supplier of the electrochemical bias, and the CO<sub>2</sub> conversion takes place on an electrode wired to the PV cell.<sup>63</sup> The separation of the optical and electrical components allows a greater selection of materials and eliminates concerns of processing compatibilities and solution stability of the light-active components. Furthermore, in principle, it allows the use of high-quality (and expensive) electrocatalysts, because of the much higher operational current densities. This strategy has

been successfully applied for water splitting to produce hydrogen. The price of renewable hydrogen has dropped to about €3.23 kg<sup>-1</sup> considering the parameters relevant to Germany, which is already competitive with small and medium-size operations of conventional, fossil fuel-based processes. Considering the trend in the cost, €2.50 kg<sup>-1</sup> seems realistic within a decade, which will be competitive with petrochemical approaches.<sup>63</sup> We envision similar opportunities for PV+EC CO<sub>2</sub> conversion, once mature electrolyzer technologies will be available.

*Performance Metrics for PS/PC, PEC, and PV+EC Approaches.* As data-mining becomes a major component of every research project, it is now more important than ever to report experimental data (and the drawn conclusions) in a manner that comparisons among laboratories can be easily made.<sup>68</sup> While analyzing the papers from the past 5 years, we collected a broad set of performance metrics (Table 2), to see which ones allow the most meaningful comparisons for PS/PC, PEC, and PV+EC studies.

Activity, selectivity, and durability are usually the main three aspects to evaluate the performance of different solar-driven CO<sub>2</sub> conversion approaches. In PS/PC studies, product formation rate is the most commonly reported metric for evaluating the activity. In most cases, the formation rate is normalized over the weight of the catalyst or the geometrical area if it is immobilized on a substrate. Products, however, may vary in different catalytic systems. It is a worthwhile exercise to normalize the formation rate with the reaction stoichiometry (i.e., numbers of electrons transferred in the reaction); thus, comparisons can be reasonably made among different products (such analysis will be shown later). Quantum efficiency (QE) is another important component of the light-to-fuel efficiency,



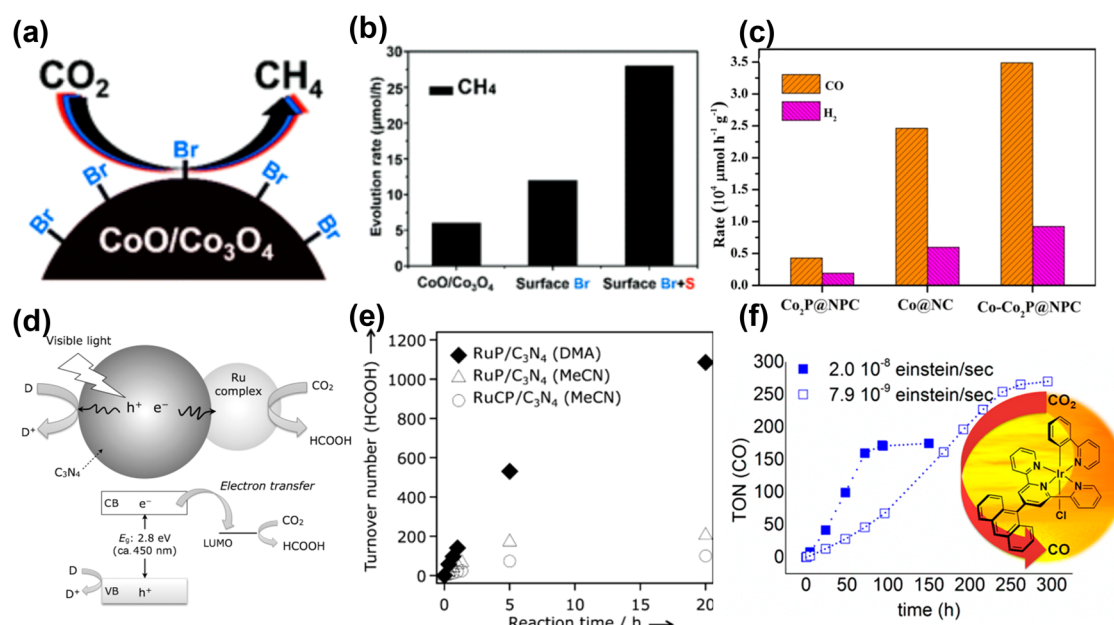


Figure 3. (a) Schematic illustration of N-bromosuccinimide treated cobalt oxide nanoparticles and (b)  $\text{CH}_4$  formation rate over catalysts with different surface treatments. Reprinted with permission from ref 99. Copyright 2019 Royal Society of Chemistry. (c) Comparison of  $\text{CO}_2$  reduction performances of different catalysts. Reprinted with permission from ref 102. Copyright 2019 Wiley-VCH. (d) Schematic illustration of  $\text{CO}_2$  reduction using a  $\text{Ru}$  complex/ $\text{C}_3\text{N}_4$  hybrid photocatalyst and (e) the turnover number of  $\text{HCOOH}$  production as a function of irradiation time using different photocatalysts and solvents. Reprinted with permission from ref 103. Copyright 2019 Wiley-VCH. (f) The turnover number of  $\text{CO}$  evolution as a function of irradiation time over modified iridium(III) photocatalyst. Reprinted from ref 104. Copyright 2017 American Chemical Society.

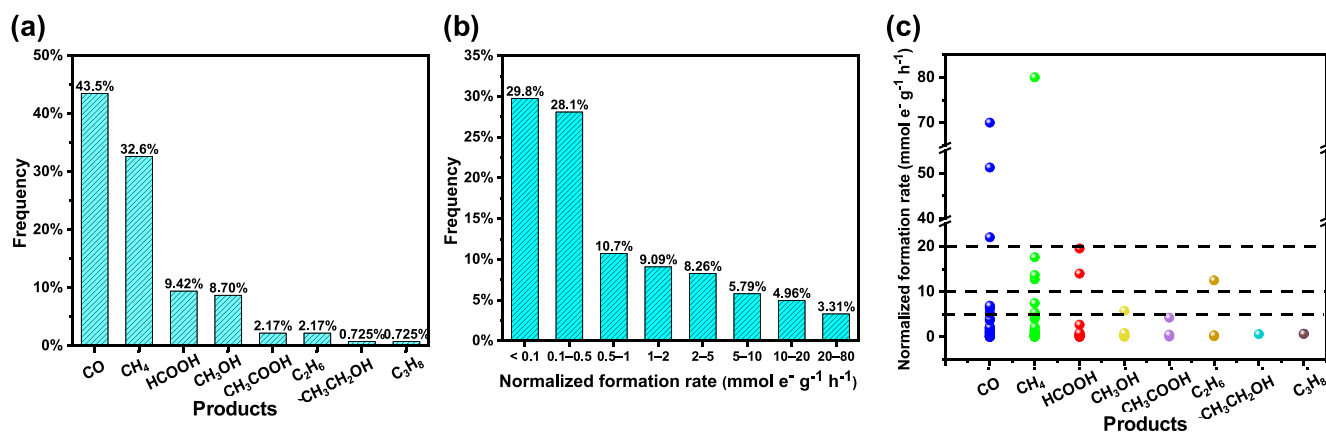


Figure 4. Statistical analysis of PS/PC  $\text{CO}_2$  conversion studies: (a) product distribution, (b) normalized formation rate distribution, and (c) normalized formation rate distribution of different products.

but it is not provided in all reports. For the PEC approach, the Faradaic efficiency (FE) is the most reported metric, often misleadingly interpreted as an activity descriptor. In addition, the onset potential of the reduction process (the potential/voltage at which the product detection measurement was carried out) and the corresponding normalized current density are also important metrics to be reported. Solar-to-fuel conversion efficiency (SFE) is a key metric, which is less reported in PEC systems. Strictly speaking, SFE is applicable only if no external bias is employed. Incident photon-to-current conversion efficiency (IPCE) and absorbed photon-to-current conversion efficiency (APCE) can also reflect the efficiency from different aspects.<sup>69</sup> In PV+EC related systems, the performance metrics are similar to those of the PEC. The

operation points (including voltage and current density) are usually provided, and SFE is more commonly reported.

**Recent Development in PS/PC  $\text{CO}_2$  Conversion.** In the past 5 years, numerous research articles have been published focusing on further improving the activity, selectivity, and durability for PS/PC  $\text{CO}_2$  reduction. There are also a lot of reviews and perspectives, such as a summary of photocatalyst development,<sup>7,8,16,20–22,24,27,28,70–91</sup> design strategies for reactors,<sup>18,92,93</sup> and the possibilities and challenges of solar fuel production.<sup>8,14,17,19,27,28,94–98</sup> Here, we highlighted three studies on PS and PC  $\text{CO}_2$  conversion with outstanding performance in some regard (see bold values in Table 3).

$\text{CO}_2$  reduction to  $\text{CH}_4$  with high formation rate and selectivity was reported, when surface activated cobalt oxide nanoparticles were used as catalyst.<sup>99</sup> As shown in Figure 3a,

Table 4. Selected Studies on PEC CO<sub>2</sub> Conversion

Photocathode–Dark Anode									
cathode	anode	illumination conditions	electrolyte	potential and current density	products	FE (%)	SFE (%)	maximum test time (h)	ref
Bi Nanosheets	Graphite	1 Sun	NaHCO <sub>3</sub>	−1.1 V vs RHE, 18 mA cm <sup>−2</sup>	HCOOH	~100	1.5	12	105
In <sub>0.4</sub> Bi <sub>0.6</sub> /MAPbI <sub>3</sub>	Pt	1 Sun	KHCO <sub>3</sub>	−0.6 V vs RHE, ~5.5 mA cm <sup>−2</sup>	HCOOH	~100		1.5	106
TiO <sub>2</sub> -protected Cu <sub>2</sub> O–Re(tBu-bipy)(CO) <sub>3</sub> Cl	Pt	Xe lamp with KG 3 and AM 1.5 G filters	Re(tBu-bipy)(CO) <sub>3</sub> Cl and MeOH	−1.73 V vs Fc <sup>+</sup> /Fc, ~1.5 mA cm <sup>−2</sup>	CO	~100		5.5	107
Li-doped CuFeO <sub>2</sub>	Graphite	1 Sun	pyridine acetate buffer	−0.63 V vs SCE, ~0.6 mA cm <sup>−2</sup>	CH <sub>3</sub> OH	96.7		1.5	108
CuFeO <sub>2</sub> /CuO	Pt	1 Sun	KHCO <sub>3</sub>	0.15 V vs RHE, ~1.5 mA cm <sup>−2</sup>	HCOOH	>90	1–1.2	7 days	109
Photoanode–Dark Cathode									
cathode	anode	illumination condition	electrolyte	potential and current density	products	FE (%)	SFE (%)	maximum test time (h)	ref
Pd/C-coated Ti mesh	GaAs/InGaP/TiO <sub>2</sub> /NiO <sub>x</sub>	1 Sun	Anolyte: KOH; catholyte: KHCO <sub>3</sub>	Cathode: ~−0.8 V vs Ag/AgCl, 8.5 mA cm <sup>−2</sup>	HCOOH	>94	~10	3	9

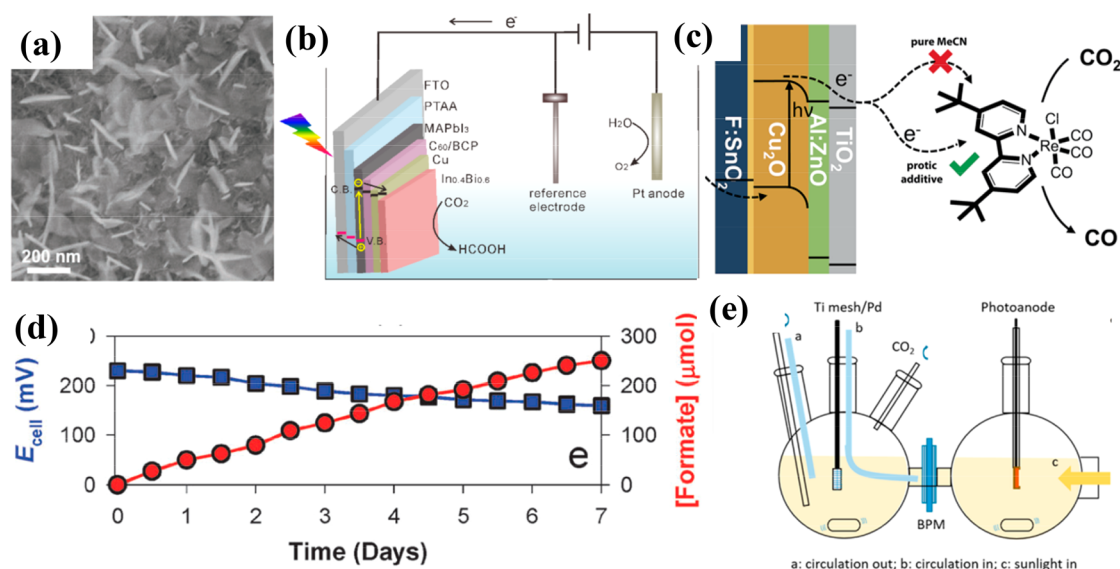


Figure 5. (a) SEM image of reduced mesoporous Bi nanosheets. Reprinted with permission from ref 105. Copyright 2018 Wiley-VCH. (b) Full cell configuration containing In<sub>0.4</sub>Bi<sub>0.6</sub>-coated perovskite photocathode. Reprinted from ref 106. Copyright 2019 American Chemical Society. (c) Schematic of the PEC CO<sub>2</sub> reduction process involving protected Cu<sub>2</sub>O photocathodes and a Re-based molecular catalyst. Reprinted with permission from ref 107. Copyright 2015 Royal Society of Chemistry. (d) Changes in  $E_{\text{cell}}$  and HCOOH production with a wired CuFeO<sub>2</sub>/CuO and Pt couple under illumination without external bias. Reprinted with permission from ref 109. Copyright 2015 Royal Society of Chemistry. (e) The scheme of photoanode-dark anode configuration for CO<sub>2</sub> conversion. Reprinted from ref 9. Copyright 2016 American Chemical Society.

treatment with N-bromosuccinimide resulted in the formation of Co<sub>3</sub>O<sub>4</sub> with coordinated Br on the surface, therefore enhancing the catalytic efficiency. The formation rate of CH<sub>4</sub> was further enhanced by surface modification with sulfur, reaching 10 mmol g<sup>−1</sup> h<sup>−1</sup> (normalized formation rate of 80 mmol e<sup>−</sup> g<sup>−1</sup> h<sup>−1</sup>) with a QE of 2.3% at 405 nm and a selectivity of 98% (Figure 3b). In another study, a heterogeneous hybrid catalyst of Co and Co<sub>2</sub>P nanoparticles was embedded in carbon nanolayers codoped with N and P (activities shown in Figure 3c) which was combined with a homogeneous Ru-based complex photosensitizer, allowing high CO formation rate.<sup>102</sup> In atomically thin layers of sulfur-deficient CuIn<sub>3</sub>S<sub>8</sub> (containing charge-enriched Cu–In dual sites), the formation of a stable Cu–C–O–In intermediate at the Cu–In dual sites was the key feature

determining selectivity.<sup>100</sup> As a result, the CuIn<sub>3</sub>S<sub>8</sub> single-unit-cell layers achieved nearly 100% selectivity for visible-light-driven CO<sub>2</sub> reduction to CH<sub>4</sub>, with a formation rate of 8.7 μmol g<sup>−1</sup> h<sup>−1</sup>. A hybrid system of a ruthenium complex and carbon nitride (C<sub>3</sub>N<sub>4</sub>) was shown to selectively convert CO<sub>2</sub> to HCOOH (Figure 3d,e).<sup>103</sup> As for molecular systems, terpyridine modifications of an iridium(III) photocatalysts with a combined 2-phenylpyridine (ppy) and 2,2′:6′,2′′-terpyridine (tpy) ligand have been investigated and yielded a turnover number (TON) of up to 265 with a QE of 0.10 (Figure 3f).<sup>104</sup> It is worth pointing out that this catalytic system showed high durability (over 10 day operation without obvious decay of activity).

To get a statistically validated picture of PS/PC CO<sub>2</sub> conversion studies, 138 cases were analyzed among those

papers published since 2014. The selection criterion was the availability of two or more of the important performance indicators in the study. The majority of these studies (>100) employed various sacrificial agents; therefore, they belong to the PC category. The results are shown in Figure 4. For the product distribution, only the major products (selectivity > 30%) of each study were counted. The most common products formed are CO and CH<sub>4</sub>, which together account for over 75% of the major products. In addition, HCOOH and CH<sub>3</sub>OH also represent 9.4% and 8.7%, respectively. Other products, such as CH<sub>3</sub>COOH, C<sub>2</sub>H<sub>6</sub>, CH<sub>3</sub>CH<sub>2</sub>OH, and C<sub>3</sub>H<sub>8</sub>, were seldom reported as major products, which is consistent with the results in the selected studies we have highlighted. To transparently compare the activity of the catalysts in these studies, the reported formation rates have been normalized with the electron-transfer number of the given product, enabling comparisons among different products. Among the above 138 cases, 121 demonstrated unambiguous formation rate data, which were selected for the subsequent analysis. As shown in Figure 4b, the formation rates concentrated within a lower range of 0–0.5 mmol e<sup>−</sup> g<sup>−1</sup> h<sup>−1</sup>, accounting for about 50% of the studies. There are 4 cases reported formation rates ranging from 20 to 80 mmol e<sup>−</sup> g<sup>−1</sup> h<sup>−1</sup>. We further analyzed the normalized formation rate distribution of different products (Figure 4c and Table S1). Only CO and CH<sub>4</sub> have been produced with a formation rate greater than 20 mmol e<sup>−</sup> g<sup>−1</sup> h<sup>−1</sup>. Interestingly, although almost 10% of the cases had HCOOH as the major product, most of them reported the formation rate lower than 5 mmol e<sup>−</sup> g<sup>−1</sup> h<sup>−1</sup>. This pattern suggests that there is a greater chance of reoxidation of HCOOH to CO<sub>2</sub> (back reaction on the very same catalyst, driven by the photogenerated holes), compared to that for the gas-phase products, which rapidly move away from the catalyst surface.

**Recent Development in PEC CO<sub>2</sub> Conversion.** The number of studies employing PEC CO<sub>2</sub> conversion approach has also grown rapidly in the past 5 years. Some outstanding examples are highlighted in Table 4.

Mesoporous bismuth nanosheets have been prepared by the cathodic transformation of atomic-thick bismuth oxycarbonate nanosheets, which showed selective CO<sub>2</sub> reduction to HCOO<sup>−</sup> with high current density (−1.1 V vs RHE, ~18 mA cm<sup>−2</sup>, FE ~100%) and operation stability (12 h). Moreover, Bi nanosheets were integrated with Ir/C dark anode in full cells and achieved a solar-to-formate conversion efficiency of 1.5%. The CO<sub>2</sub> reduction performance was rationalized by the 2D mesoporous nanosheet morphology with an enlarged surface, abundant under-coordinated Bi sites, and structural robustness (Figure 5a).<sup>105</sup>

The application of hybrid organic–inorganic and fully inorganic perovskites in PEC processes has also been a hot topic. For example, a novel photocathode was prepared by coating an In<sub>0.4</sub>Bi<sub>0.6</sub> alloy layer on a MAPbI<sub>3</sub> PV cell (as illustrated in Figure 5b), which achieved a current density of 5.5 mA cm<sup>−2</sup> at −0.6 V vs RHE, producing HCOOH at nearly 100% FE for 1.5 h.<sup>106</sup> A TiO<sub>2</sub>-protected Cu<sub>2</sub>O photocathode

The selectivity toward a given product is affected more by the electrode material and the PEC condition, rather than the product itself.

was paired with a molecular rhenium bipyridyl catalyst. At −1.73 V vs Fc<sup>+</sup>/Fc, the system showed a current density of ~1.5 mA cm<sup>−2</sup> and FE<sub>CO</sub> of nearly 100% (Figure 5c).<sup>107</sup> This kind of configuration is not a standard PEC system as we discussed above because the light absorber and active sites are

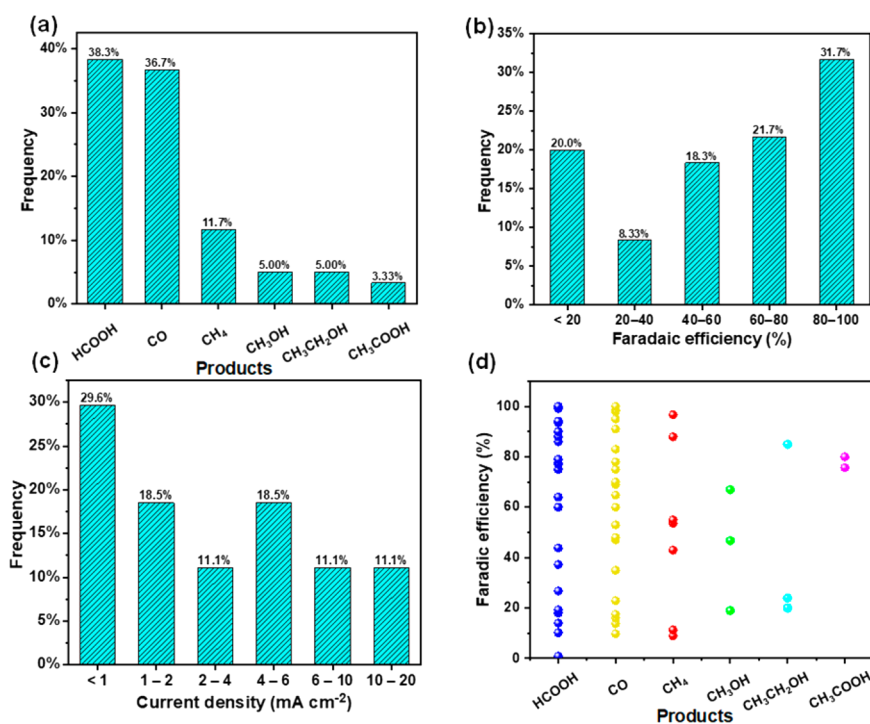


Figure 6. Statistical analysis of PEC CO<sub>2</sub> conversion studies: (a) product distribution, (b) FE distribution, (c) current density (under 1 Sun) distribution, and (d) FE distribution of different products.

Table 5. Representative Studies on PV+EC CO<sub>2</sub> Conversion

light absorber	anode	cathode	illumination conditions	electrolyte	products	operation point	FE (%)	SFE (%)	maximum test time (h)	ref
GaInP/GaInAs/Ge	CuO/SnO <sub>2</sub>	CuO/SnO <sub>2</sub>	1 Sun	Anolyte: CsOH, Catholyte: CsHCO <sub>3</sub>	CO	2.38 V, −0.55 V vs RHE, 11.6 mA cm <sup>−2</sup>	81	14.4	5	111
GaInP/GaInAs/Ge	Sr <sub>2</sub> GaCoO <sub>3</sub>	Ag	1 Sun	NaNO <sub>3</sub>	CO	2.26 V, 3.54 mA cm <sup>−2</sup>	85–89	15.6	19	112
Triple-junction GaAs (InGaP/GaAs/Ge) solar cell	Zn	Au	1 Sun	Anolyte: KOH with zinc acetate, catholyte: KHCO <sub>3</sub>	CO	1.96 V, 10 mA cm <sup>−2</sup>	~92	~16.9	24	113
GaInP/GaInAs/Ge	Ni or Pt	Ag/ GDE	1 Sun	Anolyte: KOH; Catholyte: KOH	CO	2.23 V, −0.6 V vs RHE, 14.4 mA cm <sup>−2</sup>	~100	19.1	150	114

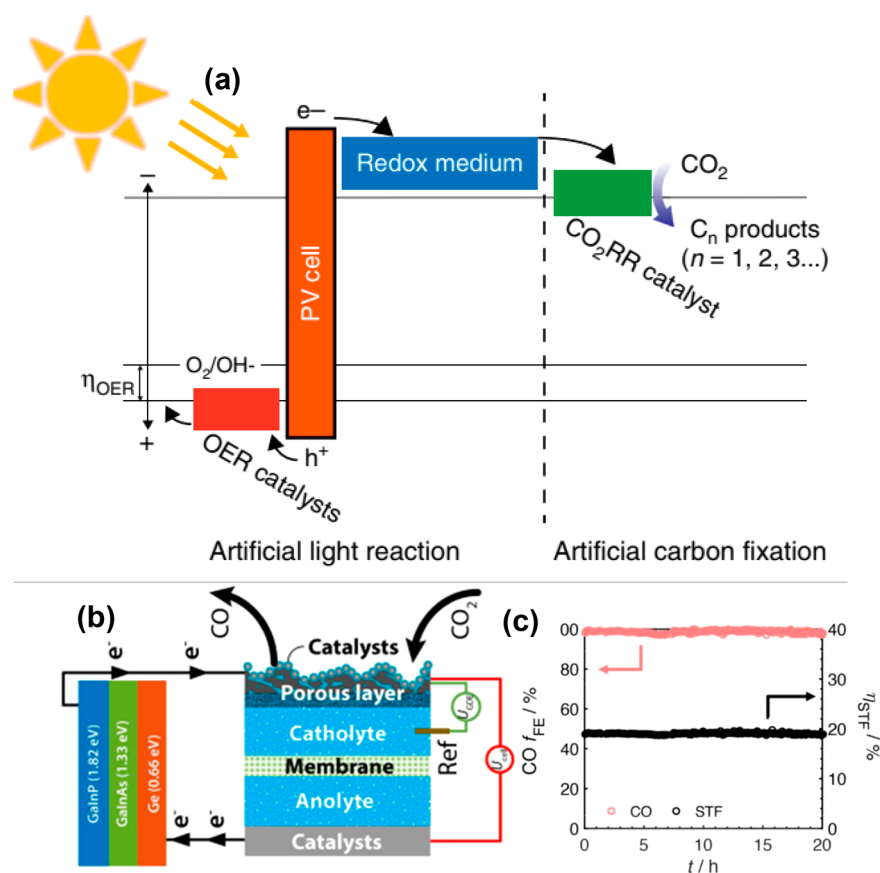


Figure 7. (a) Energy diagram of each part in a redox-medium-assisted system. Reprinted with permission from ref 113. Copyright 2018 Springer Nature. (b) Illustration of a wire connection between the triple-junction cell and GDE cell and (c) CO Faradaic efficiency and solar-to-fuel efficiency over 20 h duration. Reprinted from ref 114. Copyright 2020 American Chemical Society.

separated, and the buried junction together with the external electric power provides the bias.

There are also reports on PEC CO<sub>2</sub> reduction to alcohols, for example, CH<sub>3</sub>OH was synthesized at a Li-doped CuFeO<sub>2</sub> thin-film photocathode with a FE<sub>CH<sub>3</sub>OH</sub> of 96.7% at −0.63 V vs SCE.<sup>108</sup> Durability is another objective of the studies: a PEC cell, containing CuFeO<sub>2</sub>/CuO photocathode and Pt anode couples, could produce HCOOH for over 1 week at a solar-to-formate energy conversion efficiency of ~1% (FE > 90%) without any external bias (Figure 5d).<sup>109</sup> CuFeO<sub>2</sub>/CuO bulk heterojunction films were also capable of converting CO<sub>2</sub> into C1–C6 aliphatic acid anions under simulated sunlight in the absence of any sacrificial chemicals or electrical bias, which shows that larger molecules can also be formed via PEC C–C

coupling.<sup>110</sup> The photoanode–dark cathode configuration has also been heavily investigated. For example, a solar-driven CO<sub>2</sub> reduction cell was constructed encompassing a tandem GaAs/InGaP/TiO<sub>2</sub>/Ni photoanode, a Pd/C nanoparticle-coated Ti mesh cathode,<sup>9</sup> and a bipolar membrane to allow for steady-state operation with a separate catholyte and anolyte. At the operational current density of 8.5 mA cm<sup>−2</sup> without external bias, the cathode exhibited <100 mV overpotential and >94% FE for the reduction of CO<sub>2</sub> to formate with SFE as high as 10%.

What is common in most of the highlighted studies is the very high selectivity. Note that almost 100% FE was reported for three different products (CO, HCOOH, and CH<sub>3</sub>OH). To further elaborate on this matter, statistical analysis of the PEC CO<sub>2</sub> conversion studies has also been conducted (Figure 6).



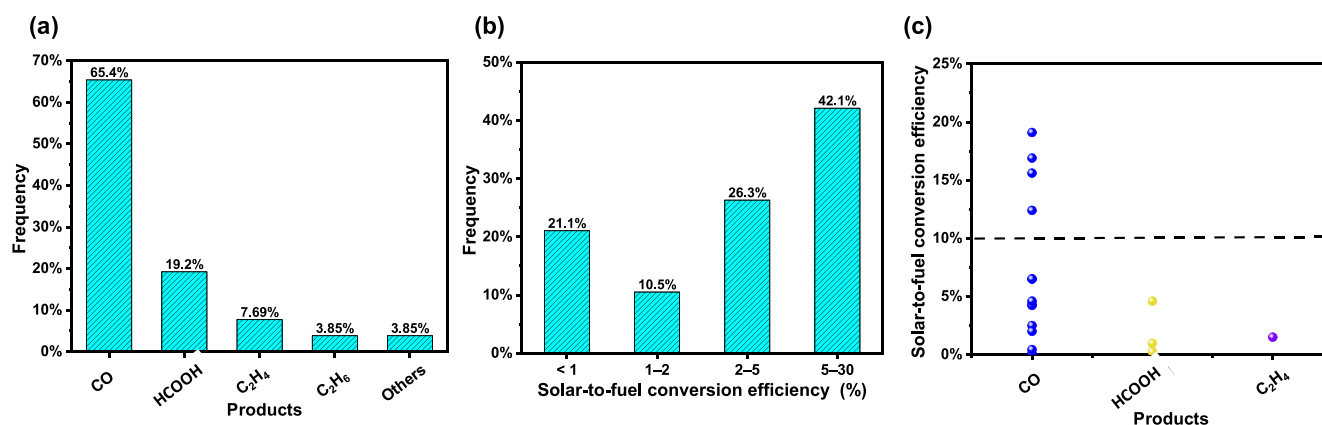


Figure 8. Statistical analysis of PV+EC CO<sub>2</sub> conversion studies: (a) product distribution, (b) SFE distribution, and (c) SFE distribution of different products.

Sixty cases were collected that provided clear FE data for corresponding CO<sub>2</sub> conversion products, which is employed as the key metric for comparing the PEC behavior herein.

For product distribution, HCOOH and CO are the most common major products reported, together accounting for 75% of the studies, followed by CH<sub>3</sub>OH (11.7%), CH<sub>4</sub> (5%), CH<sub>3</sub>CH<sub>2</sub>OH (5%), and CH<sub>3</sub>COOH (3.33%), which is consistent with the results of the highlighted studies. For the FE of the product formed in the largest amount, most of the studies reported FE higher than 60%, in which there are 32% with FE higher than 80%. There are still 20% of the studies reported, with FEs lower than 20%. To compare the activity, we also analyzed the current density distribution. More than 45% of the studies reported current density lower than 2 mA cm<sup>-2</sup>, while only 11% reported higher than 10 mA cm<sup>-2</sup>. For the FE distribution for different products, we do not see any cluster formation, which means that none of the products tends to form more selectively than others. In fact, there is a rather even distribution of the FE values for all products, which suggests that the selectivity of a given product is affected more by the electrode material and the PEC condition, rather than the product itself. It is easy to understand that different electrode materials greatly affect the product because the reducing power of the electrons in the PEC system is defined by the conduction band energy of the photocathode. The PEC condition, such as the electrolyte, also affect the surface chemistry and the intermediate species. Note that similarly high FE values were found for the highly reduced products (e.g., CH<sub>3</sub>OH, C<sub>2</sub>H<sub>5</sub>OH, CH<sub>4</sub>, etc.) to those obtained for CO and HCOOH. The detailed product distribution of PEC CO<sub>2</sub> conversion studies within different FE ranges is shown in Table S2.

**Recent Development in PV+EC CO<sub>2</sub> Conversion.** Based on the successful H<sub>2</sub> evolution studies employing PV+EC systems, this configuration has attracted much attention also for CO<sub>2</sub> reduction, especially in the past two years. Here we must make a distinction between (i) integrated systems, where the two functions are incorporated in the same unit, and those (ii) coupled ones, where regular PV panels are DC–DC connected to regular electrochemical cells. In our analysis, only the integrated systems were considered to ensure a fair comparison with the PS/PC and PEC approaches. In Table 5, we highlight some representative studies with high SFE and/or durability.

Atomic layer deposition of SnO<sub>2</sub> was performed on CuO nanowires for narrowing the product distribution of CO<sub>2</sub>

reduction, thus yielding predominantly CO. The prepared catalyst was employed as both the cathode and anode for complete CO<sub>2</sub> electrolysis. In the resulting device, the electrodes were separated by a bipolar membrane, and a GaInP/GaInAs/Ge photovoltaic cell was used to drive the solar-driven splitting of CO<sub>2</sub> into CO and oxygen with a solar-to-CO efficiency of 13.4% and overall SFE of 14.4%. The operating current density, selectivity toward CO, and solar-to-CO efficiency remained almost stable during 5 h of electrolysis.<sup>111</sup> In another study, a CO<sub>2</sub> reduction system was integrated, achieving an average solar-to-CO efficiency of 13.9% and SFE of 15.6% with no appreciable performance degradation in 19 h of operation.<sup>112</sup>

In another example, a two-step, redox-medium-assisted solar-driven CO<sub>2</sub> electroreduction system was developed by incorporating a Zn/Zn(II) redox mediator that acts as the electron carrier during the photosynthesis. In the light reaction, the solar-driven oxygen evolution and Zn(II) reduction store electrons in the Zn/Zn(II) medium. The carbon fixation releases the stored electrons and leads to an unassisted electrochemical reduction of CO<sub>2</sub>. The energy diagram of each reaction part is shown in Figure 7a.<sup>113</sup> This redox-medium-assisted system enables a solar-to-CO conversion efficiency of 15.6% under 1 Sun illumination. In addition, in a very recent study, solar-driven CO<sub>2</sub> reduction to CO with 19% solar-to-CO efficiency under 1 Sun illumination in a gas diffusion electrode (GDE) flow cell has been reported.<sup>114</sup> The use of a reverse assembled GDE (Figure 7b) prevented transition from a wetted to a flooded catalyst bed and allowed the device to operate stably for >150 h with no loss in efficiency. The FE<sub>CO</sub> and SFE over a 20 h duration are shown in Figure 7c.

As also highlighted by one of the Reviewers, the relative surface areas of PV and EC components are often significantly different, but this is often not clearly explained in the papers. In a practical device, the PV cells with a much larger area will be required compared to the area of the EC component, because of the relatively low energy density of solar irradiation. Importantly, an EC component can be cost-effective when it is smaller and runs at higher current densities (such as those with GDE cells). This mismatch, however, can bring confusion to the readers if the reported values are not concise. There have been some bad practices in reporting current density and SFE in the PV+EC systems. PV cells with a much larger area were integrated with electrodes with a smaller area, while the current density was improperly normalized with the area of the

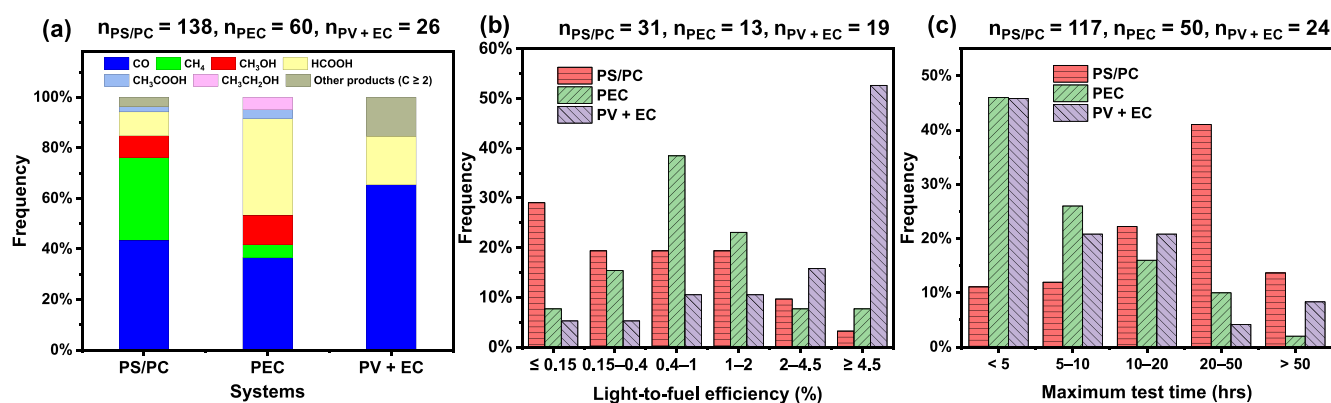


Figure 9. Comparisons of (a) product distribution, (b) light-to-fuel conversion efficiency, and (c) longest measurements in PS/PC, PEC, and PV+EC systems.

electrodes, resulting in misleadingly large current densities or SFEs. On the other hand, it is also possible to use electrodes with an area larger than that of the PV cells, especially when using expensive PV cells and relatively cheap electrode materials. In these cases, the overpotential can be very small, because of operating at low current density. Finally, in some cases the SFE was obtained under irradiance significantly lower than 1 Sun, resulting in higher SFE values, which is unlikely to scale with the light intensity.

The above highlighted studies all reported CO as the main product with high SFEs. As for the statistics, 26 cases were collected, in which 19 cases demonstrated clear SFEs (Figure 8). For the product distribution, CO is the most common product, accounting for 65.4% alone. It is followed by HCOOH with 19.2%. Most of the studies reported SFE greater than 5%, accounting for 42.1%. Only 21.1% of the cases reported SFE less than 1%. For those reporting SFEs greater than 10%, all the main products are CO, which are highlighted in the above discussion. The statistical data is shown in Table S3.

*Comparisons of the Key Performance Metrics between PS/PC, PEC, and PV+EC Approaches for Solar-Driven CO<sub>2</sub> Conversion.* We have not found any literature precedence that compared the performance metrics among different approaches for solar-driven CO<sub>2</sub> reduction. These subdisciplines, however, cannot be considered as isolated fields, and their comparison is of great importance to analyze intrinsic differences and similarities. As demonstrated in the above sections, there are different performance metrics for PS/PC, PEC, and PV+EC systems, among which, product distribution, light-to-fuel conversion efficiency, and maximum test time were selected as the indicators of selectivity, activity, and durability, respectively.

Inclusion and exclusion criteria:

- (i) Product Distribution.** The inclusion criterion follows that of the above statistical studies: only the major products (selectivity > 30%) of a given study were counted.
- (ii) Light-to-fuel Efficiency.** In principle, the cases included in the product distribution analysis were included here except those that did not provide clear light-to-fuel conversion efficiency data. In many PS/PC studies, measurements were performed under monochromatic illumination making the efficiency metrics higher than that measured under simulated sunlight or full-arc

illumination. These issues, however, had only a negligible effect on the comparison, as shown in the following discussion. Those studies using sacrificial agents in the performance evaluation were excluded in the comparison of light-to-fuel efficiency, to ensure that water oxidation is the other half reaction. For PEC studies, only studies without external bias were taken into account in the light-to-fuel conversion efficiency comparison. For PV+EC studies, SFE (or light-to-fuel efficiency in some cases) data were already obtained in the above sections.

- (iii) Maximum Reported Test Time.** All cases were included here except those that did not provide clear maximum test time data.

The comparison of product distribution is shown in Figure 9a. Overall, the products of PS/PC and PEC studies are more broadly distributed than those in PV+EC studies with a distinctly higher frequency of CO. The reason for this is that most of the PV+EC studies are proof of concept focusing on device fabrication or system validation, using commercial electrocatalysts, such as Ag<sup>115</sup> and Au<sup>116</sup> on which selective CO<sub>2</sub> reduction to CO has been widely reported. The gas products (mainly CO and CH<sub>4</sub>) together account for nearly 80% in PS/PC studies, while they account for only about 40% in PEC studies, which might be associated with the factor that in PS/PC systems, both reduction and oxidation happen on the same particle, while in PEC systems they are spatially separated. The unfavored generation of liquid products in the PS/PC system may be plausibly further consumed by the photogenerated holes involving oxidation reaction conducted at the same particle surface. In addition, the frequency of HCOOH in PS/PC studies is lower than those of PEC and PV+EC plausibly because HCOOH, as one of the thermodynamically prior products, might be oxidized by the photogenerated holes or derived oxidizing intermediates, whereas this process is avoided to a great extent in PEC and PV+EC systems.

The activities of the three approaches are compared by light-to-fuel efficiencies, as shown in Figure 9b. The differences are striking! Most of the light-to-fuel efficiencies in PS studies (PC were not included in this analysis) are located in low-value ranges, with 29.0% located between 0 and 0.15% and 19.4% located between 0.15 to 0.4%, accounting for 48.4% together. For the PEC studies, the majority is less than 2%, accounting for 61.6%. While for that of PV+EC, the light-to-fuel efficiencies are more concentrated in the high-value range

( $\geq 4.5\%$ ). There is an obvious trend that PS studies frequently reported relatively lower light-to-fuel efficiencies while those of PEC are somewhat higher, and those of PV+EC are further improved.

For the comparison of durability (shown in Figure 9c), most of the PEC and PV+EC studies reported the longest measurement with the maximum test time less than 10 h, accounting for more than 50%. Although fewer cases reported more than 50 h of durability, some of those still have good stability. Moreover, we found that PS/PC studies reported a higher frequency of more than 20 h durability. Generally, the instability in PS/PC systems is caused by photocorrosion resulting from the reduction/oxidation of the photoactive material by photogenerated electrons and holes. For that of PEC systems, not only photocorrosion but also electrocorrosion and electrolyte degradation are considerable challenges for long-term durability. The lack of many long-duration PV+EC studies is somewhat surprising, because PV cells have a very long lifetime, while over 100–1000 h stability was also demonstrated for EC systems. We speculate that more work has to be done on the integration to realize achievable durability for the combined system.

For the sake of simplicity, we compare the most important descriptors behind these trends in Table 6. As seen, the reasons are complex and convoluted; therefore, at this point, we discuss only one overarching aspect of all these areas, namely, the timescale of the different elementary processes. In Figure 10, we present the typical timescale of photoinduced processes occurring in semiconductors and at semiconductor interfaces. Most importantly, the timescale of the chemical reactions (especially the  $\text{CO}_2$  reduction reactions involving multi-electron and multiproton transfer) is in the microsecond-to-second regime. This means that a substantially long (photo)-electron lifetime is necessary for this process. Unfortunately, charge carrier recombination occurs at a much faster timescale (depending on the mechanism from subpicosecond to microsecond). This mismatch already indicates that high light-to-fuel conversion efficiencies cannot be realistically expected from PS and PEC systems, unless cocatalysts can be found, which can properly “store” electrons. There is precedence in the literature, where complex PS/PC assemblies allowed charge carrier lifetime on the order of microseconds.<sup>117</sup> This lifetime enabled different redox reactions, although not those involving the transfer of multiple electrons and protons. Specifically, in a recent study on  $\text{CsPbBr}_3$  perovskite, nanocubes facilitated photodriven C–C coupling, where both charge carriers were rapidly ( $\sim 50$  ps) extracted from the photoexcited perovskite NCs to reactant molecules. The separated charge carriers lived for more than  $0.8 \mu\text{s}$ , enabling a radical mechanism to form the C–C bonds.<sup>118</sup> At the same time, corrosion processes are also induced in the semiconductors via charge carrier trapping, posing a great threat for PS and PEC methods.<sup>119</sup> Such corrosive processes inside the semiconductors are typically faster than the  $\text{CO}_2$  reduction reaction, where charge transfer is required from the electrode surface to the substrate. This is not the case for the PV+EC method, where charge carriers are rapidly extracted from the PV cell (on the nanosecond–picosecond) timescale.

Finally, we also found that often different products formed via the different approaches even with similar catalysts. Taking  $\text{Cu}_x\text{O}$ -based catalysts as an example, several studies are listed in Table 7. There is a variety of products including  $\text{CO}$ ,  $\text{CH}_4$ ,  $\text{C}_2\text{H}_4$ ,  $\text{C}_2\text{H}_6$ ,  $\text{HCOOH}$ ,  $\text{CH}_3\text{COOH}$ , and  $\text{CH}_3\text{OH}$ . In PS and

Table 6. Summary of the Differences among PS/PC, PEC, and PV+EC Systems from Six Aspects

	PS/PC systems	PEC systems	PV+EC systems
Light absorption	One or more light absorbers are needed (see tandem and z-scheme configurations).	Either one (photocathode or photoanode) or two photoactive electrodes. The individual photoelectrodes can also be multicomponent.	Tailored photovoltaic cells can be designed (from single- to multijunction cells), to provide the necessary cell voltage.
Charge carrier collection	No need for carrier collection, but photogenerated holes and electrons need to reach the respective surface sites.	Charge carrier trapping at defect sites at the electrode/electrolyte interface hinders charge carrier collection.	Rapid charge carrier collection is achieved in the PV cell.
Charge transfer (reaction)	Both reactions proceed on the same particles. Preferably different sites for the two half reactions. Back reactions are possible. The rates of the two half reactions have to match.	Slow charge carrier transfer to the substrate or mediator from the electrode surface, compared to the timescale of charge carrier recombination.	A separate electrochemical interface is responsible for the chemical reaction. Well-known stable and active electrocatalysts can be employed.
Nano aspects	A high surface area is necessary to provide enough active sites for the reaction. High probability of surface recombination.	A high surface area is necessary to provide enough active sites for the reaction. High probability of surface recombination.	Nanostructured electrocatalysts can be used, without the detrimental surface recombination in the light absorber.
Stability	Intermediate stability, because of the presence of the solid/liquid interface.	Very difficult to achieve reasonable stability, because of the presence of current flow and the electrode/electrolyte interface. Different protective coatings seem to ensure certain improvements.	The stability is dictated only by the stability of the electrolyzer, as PV panels are stable for ages. Examples on the order of hundreds of hours are available.
Cost	Cheap experimental setup or device, but expensive multifunctional catalyst materials are needed.	More expensive and sophisticated cell designs are necessary, especially in the case of continuous flow processes. If a cocatalyst is employed, large amounts are needed because of the identical surface area of the light absorber and the electrochemical interface.	Relatively expensive system cost. Much smaller electrochemically active area is needed (compared to the size of the PV) and thus less electrocatalysts, membranes, etc. have to be used. It is also possible to select high-performance PV cells with a smaller area (under concentrated light) and electrodes with a larger area.

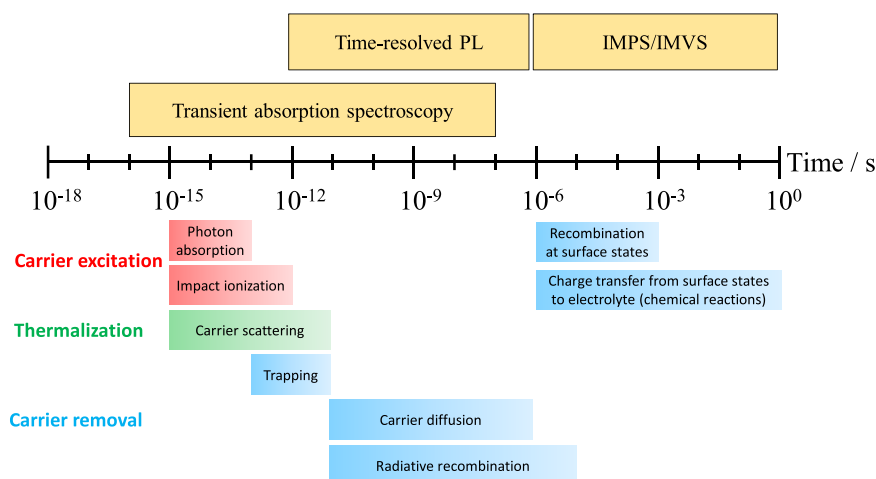


Figure 10. Typical timescale of different photoinduced processes in semiconductors, together with the methods that are employed to monitor them. PL, photoluminescence; IMPS/IMVS, intensity-modulated photocurrent/photovoltage spectroscopy.

Table 7. Representative Studies on Solar-Driven  $\text{CO}_2$  Conversion Using  $\text{Cu}_x\text{O}$ -Based Catalysts

system	catalyst	main product(s)	formation rate ( $\text{mmol e}^- \text{g}_{\text{cat}}^{-1} \text{h}^{-1}$ )	FE (%)	SFE (%)	ref
PS	carbon quantum dots/ $\text{Cu}_2\text{O}$	$\text{CH}_3\text{OH}$	0.336			121
PEC	$\text{Cu}_2\text{O}-\text{Cu}$	$\text{HCOOH}$		14		122
		$\text{CH}_3\text{COOH}$		76		123
		$\text{CH}_4$		47		124
		$\text{CH}_3\text{OH}$		53.6		125
PV+EC	$\text{CuO}$	$\text{C}_2\text{H}_4$		34		126
		$\text{C}_2\text{H}_6$		6.5		126
		$\text{CO}$			2.5	126
		$\text{HCOOH}$			0.25	126

Table 8. Representative Studies on Solar-Driven  $\text{CO}_2$  Conversion Using Au-Based Catalysts

system	catalyst	main product(s)	selectivity (%)	FE (%)	SFE (%)	ref
PS (Plasmonic catalysis)	Au	$\text{C}_1-\text{C}_3$ hydrocarbons	50% ( $\text{C}_{2+}$ hydrocarbons)			127
PEC	Cathode					
	Au/Si	$\text{CO}$		91		60
	Au/B doped $\text{g-C}_3\text{N}_4$	$\text{CH}_3\text{CH}_2\text{OH}$		47		128
PV+EC	Au	$\text{CO}$		~92	15.6	113

PEC systems, the conduction band energy of the photocathode defines the energy of the photoelectrons, while in the PV+EC systems, it is dictated by the electrode potential. This important difference also means that while in electrocatalysis the reaction rate (i.e., current density) and the reducing power of the electrons (i.e., the electrode potential) are inherently coupled (see the Butler–Volmer equation), this is not the case for PEC.<sup>120</sup> This simple fact can be a major contributor to the observed differences in the product distributions and a major opportunity for PEC-based methods in the future.

The same catalyst may play different roles in different scenarios. Taking Au-based catalysts as an example, three studies are shown in Table 8. In a PS study, Au nanoparticles (NPs) were used as a catalyst for the conversion of  $\text{CO}_2$  and  $\text{H}_2\text{O}$  into  $\text{C}_1-\text{C}_3$  hydrocarbons under visible light irradiation.<sup>127</sup> The Au NPs possess a strong localized surface plasmon resonance (LSPR) band centered around 520 nm, which enables the generation of energetic electron–hole carriers under green light for the reduction of  $\text{CO}_2$  and oxidation of  $\text{H}_2\text{O}$ , resulting in the main products of hydrocarbons. In two PEC studies, Au cocatalyst can lead to

main products  $\text{CO}$  and  $\text{CH}_3\text{CH}_2\text{OH}$  in different studies.<sup>60,128</sup> In such cases, beyond facilitating charge transfer, the cocatalyst also affects the energetics of the electrode/electrolyte interface. In the highlighted PV+EC study, the main product is  $\text{CO}$ , where Au acted as an electrocatalyst.<sup>113</sup>

At this stage only the PV+EC approach shows a performance (especially in terms of activity and durability) that can lead to industrial technologies in the near future.

**Summary.** Over the past years, the fundamental understanding of the solar-driven  $\text{CO}_2$  conversion reaction has improved substantially,<sup>129–136</sup> and deactivation mechanisms have also been studied.<sup>137,138</sup> Integration and validation of reactors and systems are also ongoing.<sup>111,114,125,139–146</sup> With this Focus Review, our aim was to provide an overview of the state-of-the-art solar-driven  $\text{CO}_2$  conversion approaches. We



have presented for the first time a statistical analysis of activity, selectivity, and durability of PS/PC, PEC, and PV+EC systems. The results indicate that (i) only the minority of studies present all those metrics, which fully describe the performance of a given system; (ii) the CO<sub>2</sub> reduction products and their distribution are different in the different scenarios, and (iii) at this stage only the PV+EC approach shows a performance (especially in terms of activity and durability), which can lead to industrial technologies in the near future (see Figure 9 and Table 6).

Based on the statistical analysis, several questions and problems were raised:

- (i) **Unbalanced research efforts.** More than 80% of the studies focused on PS/PC CO<sub>2</sub> conversion, most of which discussed catalyst synthesis and the corresponding laboratory performance evaluation. Very recently, critical comments were made on the doping of graphene with a plethora of elements for enhanced electrocatalytic effect.<sup>147</sup> We see a very similar trend in solar-driven PS/PC CO<sub>2</sub> conversion, namely that hundreds of “doped photocatalysts” are being tested with little outcome.
- (ii) **Avoid the pitfalls.** As discussed in the introduction of PC systems, many studies employ sacrificial electron donors, without evaluating the fate of these agents. It is strongly required to carry out a complete study on the overall solar-driven reactions, not only the CO<sub>2</sub> reduction half of it. Another critical issue is to confirm that CO<sub>2</sub> is the actual source of the carbon-containing products. Isotopic <sup>13</sup>CO<sub>2</sub> labeling is an efficient technique for this purpose. Quantitative detection of the evolved oxygen can also help quantifying the performance. Moreover, a control test without CO<sub>2</sub> but in the presence of H<sub>2</sub>O would be a cost-effective, yet preliminary approach to confirm/exclude participation of carbon residues (on active sites) in CO<sub>2</sub> reduction.
- (iii) **Lack of complete data set.** Only a minority of the studies contain metrics which fully describe the performance of a given system. While it is encouraging to see many studies being carried out in this area, telling the whole story is essential. This not only demonstrates the reliability of the work but also ensures reproducibility. Finally, reporting the appropriate metrics helps to make clear comparisons with other studies, shows the research status we have reached, and reminds how far we are from industrial applications.

By taking a careful look at the metrics presented above (especially concerning SFE values), we have to conclude that only the PV+EC systems have the potential to become an industrial technology in the near and midterm future.<sup>148</sup> Several trends support this notion, most importantly: (i) The rapid improvements of PCE and a decrease in the cost of PV cells. In fact, the price of solar electricity has decreased to a level that in over 20 countries translates to grid parity. (ii) The continuous progress in developing practical CO<sub>2</sub> electrolyzers.<sup>149</sup> Particularly, there are emerging trends in the employment of gas diffusion electrodes (GDEs), aiming to eliminate limitations arising from slow mass transport and small turnover number at the active sites.<sup>150,151</sup> The use of GDEs enabled the achievement of operational parameters of great industrial significance; unfortunately, not yet all of them

are for the same system. These are (i) current densities higher than 300 mA cm<sup>-2</sup>, (ii) cell voltages in the 2.5–3.0 V range (translating to energy efficiencies higher than 50%), (iii) close to 100% FE for CO and HCOOH, and (iv) over 5000 h durability.

**Future Directions.** **Selectivity** is the metric which seems to be the most addressable if we better understand the nature of active sites.<sup>152–158</sup> Atomic-level understanding of the active sites and transformation mechanisms under realistic working conditions is a prerequisite for the rational design of photoactive materials with high selectivity. For example, the (110) facet of a single-crystal Cu<sub>2</sub>O particle is active for photodriven CO<sub>2</sub> reduction to methanol while the (100) facet is inert. The oxidation state of the active sites changes from Cu(I) toward Cu(II) because of CO<sub>2</sub> and H<sub>2</sub>O coadsorption and changes back to Cu(I) after CO<sub>2</sub> conversion under visible light illumination.<sup>156</sup>

**Hybrid photoelectrode assemblies** offer a platform to rationally design materials for solar-driven CO<sub>2</sub> conversion. We need to consider the following processes. (i) Light absorption: it is essential to harness a reasonable portion of the solar spectrum. (ii) Charge transport: the semiconductor shall have high charge carrier mobility. The amount of bulk and surface traps shall also be minimized. (iii) Charge transfer kinetics: facile charge transfer from the semiconductor to either the CO<sub>2</sub> molecules in the solution, or to a mediator (either immobilized or in the solution), is required. (iv) Stability and robustness are definitely major concerns, where chemical, electrochemical, and photocorrosion all have to be considered. Considering these very complex requirements, which have to be met by a photoelectrode, it is not too surprising that no single material could meet all of these so far. In biological systems, one can find complex architectures with components that have precisely defined functionality and complementarity. As a bioinspired approach, some of the limitations of the individual components can be overcome by the rational design and assembly of hybrid PS/PC and PEC materials, where the different functionalities are decoupled. For example, CsPbBr<sub>3</sub>@zeolitic imidazolate framework nanocomposites have been reported to exhibit enhanced CO<sub>2</sub> reduction activity due to the addition of zeolitic imidazolate framework with its original CO<sub>2</sub> capturing ability and the role of acting as a cocatalyst.<sup>159</sup> In addition, it was demonstrated by the example of Cu<sub>2</sub>O that when a highly conductive scaffold is introduced into the photoelectrode, the charge carrier transport can be enhanced, and larger photocurrents can be harvested.<sup>160,161</sup> Similar trends have also been discovered in organic photoelectrodes.<sup>162</sup> This strategy greatly broadened the range of the catalyst and light absorber selection by reasonably combining the attractive features of each component.

**Nanoscale aspects** are important to enhance the current density to a level that makes practical significance. The field of nanostructured photoelectrodes is surprisingly an unexplored area. While the PS/PC<sup>163</sup> and the EC communities have built solid and coherent knowledge on the effect of catalyst size at the nanoscale, there is no systematic study on this matter for PEC processes. In fact, the long-standing theory of PEC builds on thick electrode films (with film thickness of over several micrometers).<sup>164</sup> Systematic study of nanoscale effects in PEC would be indeed important, because they affect all the important processes, such as light absorption, charge carrier transport, band bending, and charge transfer. Similar considerations are also valid for the effect of morphology.

Despite some very informative studies on Si micro-<sup>165,166</sup> and nanowires,<sup>167</sup> there is a lack of knowledge whether there is an ideal morphology for PEC applications. In addition, the consequence of drastically increased surface/bulk ratio (which is the case for nanomaterials) on the contribution of surface functional groups to the materials' property has remained unknown.

**Plasmonic catalysis** has become an emerging avenue in CO<sub>2</sub> conversion by the promise of these particles to harness visible light as hot carriers and their intrinsic catalytic activity toward CO<sub>2</sub> reduction. Noble metal NPs, in particular, allow the integration of strong visible-wavelength plasmonic excitation with surface activation of CO<sub>2</sub> and therefore represent a novel and promising class of photocatalysts for CO<sub>2</sub> reduction.<sup>8</sup> The fundamental understanding of plasmon-assisted CO<sub>2</sub> reduction processes, however, is still lacking. In plasmonic CO<sub>2</sub> reduction reaction, catalytic activity, reaction pathways, and selectivity are expected to not only depend on the properties of the metal and metal/adsorbate interactions but also possibly be tuned by light excitation.<sup>168–170</sup>

**Buried junction** is another promising approach, because if properly designed, it can integrate the benefits of PV and EC technologies.<sup>871</sup> In practice, the employment of buried junction in integrated PEC cells can overcome the instability issue. The PV components in the buried junction can act as more efficient and stable light absorbers than most of the single semiconductors when physical contact with the aqueous environment is avoided.<sup>172</sup> This strategy might provide a new direction toward the enhanced durability of PEC systems.

**Concentrated sunlight** can enable high current density operation for both the PEC and PV+EC approaches. In these cases, the solar power input can be concentrated up to 500 Suns, which in combination with proper PV cells or photoelectrodes can allow current densities similar to those in industrial electrolyzers. For water splitting, 0.88 A cm<sup>-2</sup> current density was demonstrated with an STH efficiency of over 15%, under concentrated solar irradiation (up to 474 kW m<sup>-2</sup>).<sup>173</sup> Similar integration of photoanodes or PV cells can be envisioned with CO<sub>2</sub> reduction GDEs on the cathode side. Such studies are in progress in our laboratory and will be communicated soon.

**Value-added anode processes** are also worth more consideration. Most CO<sub>2</sub> reduction approaches couple cathodic CO<sub>2</sub> reduction with the anodic oxygen evolution reaction (OER), resulting in approximately 90% of the electricity input being consumed by the OER in the EC scenario.<sup>174</sup> This issue can be addressed by coupling other anodic oxidation reactions with less electricity needs and probably higher-value products. For example, oxidation of glycerol (a byproduct of biodiesel and soap production) can lower electricity consumption up to 53%, thus reducing the operating costs and carbon footprint. In addition, value-added products can be produced, including glyceraldehyde and lactic acid.<sup>174</sup> This strategy might also offer opportunities to the PC and PEC approaches as well, because there will be no need to cope with the difficult OER, and in fact, thermodynamically downhill processes can be designed.

**PV+EC systems** can be further improved through component development, because to date, the focus was mostly on catalysts. A recent study has demonstrated that the largest voltage losses may occur at the membrane or the membrane electrode assembly rather than at the catalyst layers in their flow cell.<sup>175</sup> As another example, we note that a solid

electrolyte may be a better alternative, because the formed liquid products are in a mixture with the dissolved salts in liquid electrolytes, requiring energy-intensive downstream separation. However, in the solid electrolyte, the generated cations (such as H<sup>+</sup>) and anions (such as HCOO<sup>-</sup>) are combined to form pure product solutions without mixing with other ions.<sup>154</sup> In addition, the development of reactors for EC CO<sub>2</sub> utilization is also required, to optimize such characteristics as geometrical configuration, construction material, heat exchange, and mixing and flow characteristics.<sup>18,176</sup>

## ■ ASSOCIATED CONTENT


### Supporting Information

The Supporting Information is available free of charge at <https://pubs.acs.org/doi/10.1021/acsenerylett.0c00645>.

Statistical data of PS, PEC, and PV+EC systems (PDF)

## ■ AUTHOR INFORMATION

### Corresponding Author

Csaba Janáky – Department of Physical Chemistry and Materials Science, Interdisciplinary Excellence Centre, University of Szeged, Szeged H-6720, Hungary;  [orcid.org/0000-0001-5965-5173](https://orcid.org/0000-0001-5965-5173); Phone: +36-62-546-393; Email: [janaky@chem.u-szeged.hu](mailto:janaky@chem.u-szeged.hu)

### Author

Jie He – Department of Physical Chemistry and Materials Science, Interdisciplinary Excellence Centre, University of Szeged, Szeged H-6720, Hungary

Complete contact information is available at:

<https://pubs.acs.org/doi/10.1021/acsenerylett.0c00645>

### Notes

The authors declare no competing financial interest.

### Biographies

Dr. Jie He is a postdoctoral research fellow at the University of Szeged, Hungary. He obtained his Ph.D. from Hunan University, China in 2018. His research interest includes integration and validation of continuous flow photoelectrochemical CO<sub>2</sub> conversion cell and development of novel photoactive materials for water splitting. <https://orcid.org/0000-0001-5481-6986>

Prof. Csaba Janáky is an associate professor and Principal Investigator of the Photoelectrochemistry Research Group at the University of Szeged, Hungary. His research group focuses on converting CO<sub>2</sub> to useful chemicals, utilizing solar energy. His ERC supported activity spans through the materials aspects of photoelectrochemistry to electrochemical cell development. <https://orcid.org/0000-0001-5965-5173>

## ■ ACKNOWLEDGMENTS

This project has received funding from the European Research Council (ERC) under the European Union's Horizon 2020 research and innovation programme (Grant Agreement Nos. 716539 and 899747). This research was partially supported by the "Széchenyi 2020" program in the framework of GINOP-2.3.2-15-2016-00013 "Intelligent materials based on functional surfaces—from syntheses to applications" project. The authors thank Dr. Biborka Janáky-Bohner for her help with manuscript preparation and Prof. Krishnan Rajeshwar (UT Arlington, United States and Prof. Balázs Endrődi (University of Szeged,

Hungary) for their comments on an earlier version of the manuscript.

## REFERENCES

- (1) Jacobson, T. A.; Kler, J. S.; Hernke, M. T.; Braun, R. K.; Meyer, K. C.; Funk, W. E. Direct Human Health Risks of Increased Atmospheric Carbon Dioxide. *Nat. Sustain.* **2019**, *2* (8), 691–701.
- (2) ESRL Global Monitoring Division - Global Greenhouse Gas Reference Network. <https://www.esrl.noaa.gov/gmd/ccgg/trends/global.html> (accessed 2020-03-19).
- (3) Rogelj, J.; Den Elzen, M.; Höhne, N.; Fransen, T.; Fekete, H.; Winkler, H.; Schaeffer, R.; Sha, F.; Riahi, K.; Meinshausen, M. Paris Agreement Climate Proposals Need a Boost to Keep Warming Well below 2°C. *Nature* **2016**, *534* (7609), 631–639.
- (4) De Luna, P.; Hahn, C.; Higgins, D.; Jaffer, S. A.; Jaramillo, T. F.; Sargent, E. H. What Would It Take for Renewably Powered Electrosynthesis to Displace Petrochemical Processes? *Science* **2019**, *364* (6438), 3506.
- (5) Nørskov, J. K.; Weckhuysen, B.; Centi, G.; et al. *Research Needs towards Sustainable Production of Fuels and Chemicals*; Energy X, 2019 September. Downloaded from: [https://www.energy-x.eu/wp-content/uploads/2019/09/Energy\\_X\\_Research-needs-report.pdf](https://www.energy-x.eu/wp-content/uploads/2019/09/Energy_X_Research-needs-report.pdf).
- (6) Villadsen, S. N. B.; Fosbøl, P. L.; Angelidaki, I.; Woodley, J. M.; Nielsen, L. P.; Møller, P. The Potential of Biogas; the Solution to Energy Storage. *ChemSusChem* **2019**, *12* (10), 2147–2153.
- (7) Ran, J.; Jaroniec, M.; Qiao, S. Z. Cocatalysts in Semiconductor-Based Photocatalytic CO<sub>2</sub> Reduction: Achievements, Challenges, and Opportunities. *Adv. Mater.* **2018**, *30* (7), 1704649.
- (8) Yu, S.; Wilson, A. J.; Kumari, G.; Zhang, X.; Jain, P. K. Opportunities and Challenges of Solar-Energy-Driven Carbon Dioxide to Fuel Conversion with Plasmonic Catalysts. *ACS Energy Lett.* **2017**, *2* (9), 2058–2070.
- (9) Zhou, X.; Liu, R.; Sun, K.; Chen, Y.; Verlage, E.; Francis, S. A.; Lewis, N. S.; Xiang, C. Solar-Driven Reduction of 1 Atm of CO<sub>2</sub> to Formate at 10% Energy-Conversion Efficiency by Use of a TiO<sub>2</sub>-Protected III-V Tandem Photoanode in Conjunction with a Bipolar Membrane and a Pd/C Cathode. *ACS Energy Lett.* **2016**, *1* (4), 764–770.
- (10) Grim, R. G.; Huang, Z.; Guarnieri, M. T.; Ferrell, J. R.; Tao, L.; Schaidle, J. A. Transforming the Carbon Economy: Challenges and Opportunities in the Convergence of Low-Cost Electricity and Reductive CO<sub>2</sub> Utilization. *Energy Environ. Sci.* **2020**, *13* (2), 472–494.
- (11) Halmann, M. Photoelectrochemical Reduction of Aqueous Carbon Dioxide on P-Type Gallium Phosphide in Liquid Junction Solar Cells. *Nature* **1978**, *275*, 115–116.
- (12) Kim, W.; McClure, B. A.; Edri, E.; Frei, H. Coupling Carbon Dioxide Reduction with Water Oxidation in Nanoscale Photocatalytic Assemblies. *Chem. Soc. Rev.* **2016**, *45* (11), 3221–3243.
- (13) White, J. L.; Baruch, M. F.; Pander, J. E.; Hu, Y.; Fortmeyer, I. C.; Park, J. E.; Zhang, T.; Liao, K.; Gu, J.; Yan, Y.; Shaw, T. W.; Abelev, E.; Bocarsly, A. B. Light-Driven Heterogeneous Reduction of Carbon Dioxide: Photocatalysts and Photoelectrodes. *Chem. Rev.* **2015**, *115* (23), 12888–12935.
- (14) Tu, W.; Zhou, Y.; Zou, Z. Photocatalytic Conversion of CO<sub>2</sub> into Renewable Hydrocarbon Fuels: State-of-the-Art Accomplishment, Challenges, and Prospects. *Adv. Mater.* **2014**, *26* (27), 4607–4626.
- (15) Ulmer, U.; Dingle, T.; Duchesne, P. N.; Morris, R. H.; Tavasoli, A.; Wood, T.; Ozin, G. A. Fundamentals and Applications of Photocatalytic CO<sub>2</sub> Methanation. *Nat. Commun.* **2019**, *10* (1), 3169.
- (16) Li, C.; Tong, X.; Yu, P.; Du, W.; Wu, J.; Rao, H.; Wang, Z. M. Carbon Dioxide Photo/Electroreduction with Cobalt. *J. Mater. Chem. A* **2019**, *7* (28), 16622–16642.
- (17) Wang, C.; Sun, Z.; Zheng, Y.; Hu, Y. H. Recent Progress in Visible Light Photocatalytic Conversion of Carbon Dioxide. *J. Mater. Chem. A* **2019**, *7* (3), 865–887.
- (18) Khan, A. A.; Tahir, M. Recent Advancements in Engineering Approach towards Design of Photo-Reactors for Selective Photocatalytic CO<sub>2</sub> Reduction to Renewable Fuels. *J. CO<sub>2</sub> Util.* **2019**, *29*, 205–239.
- (19) Chang, X.; Wang, T.; Gong, J. CO<sub>2</sub> Photo-Reduction: Insights into CO<sub>2</sub> Activation and Reaction on Surfaces of Photocatalysts. *Energy Environ. Sci.* **2016**, *9* (7), 2177–2196.
- (20) Liu, X.; Inagaki, S.; Gong, J. Heterogeneous Molecular Systems for Photocatalytic CO<sub>2</sub> Reduction with Water Oxidation. *Angew. Chem., Int. Ed.* **2016**, *55* (48), 14924–14950.
- (21) Xiong, J.; Song, P.; Di, J.; Li, H. Ultrathin Structured Photocatalysts: A Versatile Platform for CO<sub>2</sub> Reduction. *Appl. Catal., B* **2019**, *256*, 117788.
- (22) Ye, L.; Deng, Y.; Wang, L.; Xie, H.; Su, F. Bismuth-Based Photocatalysts for Solar Photocatalytic Carbon Dioxide Conversion. *ChemSusChem* **2019**, *12* (16), 3671–3701.
- (23) Xia, T.; Long, R.; Gao, C.; Xiong, Y. Design of Atomically Dispersed Catalytic Sites for Photocatalytic CO<sub>2</sub> Reduction. *Nano-scale* **2019**, *11* (23), 11064–11070.
- (24) Wu, H. L.; Li, X. B.; Tung, C. H.; Wu, L. Z. Semiconductor Quantum Dots: An Emerging Candidate for CO<sub>2</sub> Photoreduction. *Adv. Mater.* **2019**, *31* (36), 1900709.
- (25) Marques Mota, F.; Kim, D. H. From CO<sub>2</sub> Methanation to Ambitious Long-Chain Hydrocarbons: Alternative Fuels Paving the Path to Sustainability. *Chem. Soc. Rev.* **2019**, *48* (1), 205–259.
- (26) Yang, J.; Guo, Y.; Lu, W.; Jiang, R.; Wang, J. Emerging Applications of Plasmons in Driving CO<sub>2</sub> Reduction and N<sub>2</sub> Fixation. *Adv. Mater.* **2018**, *30* (48), 1802227.
- (27) Sun, Z.; Talreja, N.; Tao, H.; Texter, J.; Muhler, M.; Strunk, J.; Chen, J. Catalysis of Carbon Dioxide Photoreduction on Nanosheets: Fundamentals and Challenges. *Angew. Chem., Int. Ed.* **2018**, *57* (26), 7610–7627.
- (28) Stolarczyk, J. K.; Bhattacharyya, S.; Polavarapu, L.; Feldmann, J. Challenges and Prospects in Solar Water Splitting and CO<sub>2</sub> Reduction with Inorganic and Hybrid Nanostructures. *ACS Catal.* **2018**, *8* (4), 3602–3635.
- (29) Wu, J.; Huang, Y.; Ye, W.; Li, Y. CO<sub>2</sub> Reduction: From the Electrochemical to Photochemical Approach. *Adv. Sci.* **2017**, *4* (11), 1700194.
- (30) Li, K.; Peng, B.; Peng, T. Recent Advances in Heterogeneous Photocatalytic CO<sub>2</sub> Conversion to Solar Fuels. *ACS Catal.* **2016**, *6* (11), 7485–7527.
- (31) Faber, C.; Allahverdiyeva-Rinne, Y.; Artero, V.; Baraton, L.; Barbieri, A.; Bercegol, H.; Fleischer, M.; Huynhthi, H.; Kargul, J.; Lepaumier, H.; Lopez, L.; Magnuson, A. *Solar Energy for a Circular Economy: Technological Roadmap*; SUNRISE, 2020. Downloaded from: [https://sunriseaction.com/wp-content/uploads/2020/02/Roadmap\\_February\\_2020.pdf](https://sunriseaction.com/wp-content/uploads/2020/02/Roadmap_February_2020.pdf).
- (32) EuChemS Call for Proposals: Solar-driven chemistry 2019/2020. <https://www.euchems.eu/proposals-solar-driven-chemistry/> (accessed 2020-03-19).
- (33) Yano, J.; Haber, J. A.; Gregoire, J. M.; Friebe, D.; Nilsson, A.; Houle, F. JCAP Research on Solar Fuel Production at Light Sources. *Synchrotron Radiat. News* **2014**, *27* (5), 14–17.
- (34) Kuk, S. K.; Ham, Y.; Gopinath, K.; Boonmongkolras, P.; Lee, Y.; Lee, Y. W.; Kondaveeti, S.; Ahn, C.; Shin, B.; Lee, J. K.; Jeon, S.; Park, C. B. Continuous 3D Titanium Nitride Nanoshell Structure for Solar-Driven Unbiased Biocatalytic CO<sub>2</sub> Reduction. *Adv. Energy Mater.* **2019**, *9* (25), 1900029.
- (35) Ye, J.; Yu, J.; Zhang, Y.; Chen, M.; Liu, X.; Zhou, S.; He, Z. Light-Driven Carbon Dioxide Reduction to Methane by Methanosarcina Barkeri-CdS Biohybrid. *Appl. Catal., B* **2019**, *257*, 117916.
- (36) Shen, Q.; Huang, X.; Liu, J.; Guo, C.; Zhao, G. Biomimetic Photoelectrocatalytic Conversion of Greenhouse Gas Carbon Dioxide: Two-Electron Reduction for Efficient Formate Production. *Appl. Catal., B* **2017**, *201*, 70–76.
- (37) Amao, Y.; Kataoka, R. Methanol Production from CO<sub>2</sub> with the Hybrid System of Biocatalyst and Organo-Photocatalyst. *Catal. Today* **2018**, *307*, 243–247.
- (38) Yadav, R. K.; Oh, G. H.; Park, N. J.; Kumar, A.; Kong, K. J.; Baeg, J. O. Highly Selective Solar-Driven Methanol from CO<sub>2</sub> by a



Photocatalyst/Biocatalyst Integrated System. *J. Am. Chem. Soc.* **2014**, *136* (48), 16728–16731.

(39) Yaashikaa, P. R.; Senthil Kumar, P.; Varjani, S. J.; Saravanan, A. A Review on Photochemical, Biochemical and Electrochemical Transformation of CO<sub>2</sub> into Value-Added Products. *J. CO<sub>2</sub> Util.* **2019**, *33*, 131–147.

(40) Yadav, R. K.; Baeg, J. O.; Kumar, A.; Kong, K. J.; Oh, G. H.; Park, N. J. Graphene-BODIPY as a Photocatalyst in the Photocatalytic-Biocatalytic Coupled System for Solar Fuel Production from CO<sub>2</sub>. *J. Mater. Chem. A* **2014**, *2* (14), 5068–5076.

(41) Wang, L.; Wang, Y.; Cheng, Y.; Liu, Z.; Guo, Q.; Ha, M. N.; Zhao, Z. Hydrogen-Treated Mesoporous WO<sub>3</sub> as a Reducing Agent of CO<sub>2</sub> to Fuels (CH<sub>4</sub> and CH<sub>3</sub>OH) with Enhanced Photothermal Catalytic Performance. *J. Mater. Chem. A* **2016**, *4* (14), 5314–5322.

(42) Meng, X.; Wang, T.; Liu, L.; Ouyang, S.; Li, P.; Hu, H.; Kako, T.; Iwai, H.; Tanaka, A.; Ye, J. Photothermal Conversion of CO<sub>2</sub> into CH<sub>4</sub> with H<sub>2</sub> over Group VIII Nanocatalysts: An Alternative Approach for Solar Fuel Production. *Angew. Chem., Int. Ed.* **2014**, *53* (43), 11478–11482.

(43) Jia, J.; O'Brien, P. G.; He, L.; Qiao, Q.; Fei, T.; Reyes, L. M.; Burrow, T. E.; Dong, Y.; Liao, K.; Varela, M.; Pennycook, S. J.; Hmadeh, M.; Helmy, A. S.; Kherani, N. P.; Perovic, D. D.; Ozin, G. A. Visible and Near-Infrared Photothermal Catalyzed Hydrogenation of Gaseous CO<sub>2</sub> over Nanostructured Pd@Nb<sub>2</sub>O<sub>5</sub>. *Adv. Sci.* **2016**, *3* (10), 1600189.

(44) Ha, M. N.; Lu, G.; Liu, Z.; Wang, L.; Zhao, Z. 3DOM-LaSrCoFeO<sub>6-δ</sub> as a Highly Active Catalyst for the Thermal and Photothermal Reduction of CO<sub>2</sub> with H<sub>2</sub>O to CH<sub>4</sub>. *J. Mater. Chem. A* **2016**, *4* (34), 13155–13165.

(45) Xu, M.; Hu, X.; Wang, S.; Yu, J.; Zhu, D.; Wang, J. Photothermal Effect Promoting CO<sub>2</sub> Conversion over Composite Photocatalyst with High Graphene Content. *J. Catal.* **2019**, *377*, 652–661.

(46) Ghossoub, M.; Xia, M.; Duchesne, P. N.; Segal, D.; Ozin, G. Principles of Photothermal Gas-Phase Heterogeneous CO<sub>2</sub> Catalysis. *Energy Environ. Sci.* **2019**, *12* (4), 1122–1142.

(47) Chen, G.; Gao, R.; Zhao, Y.; Li, Z.; Waterhouse, G. I. N.; Shi, R.; Zhao, J.; Zhang, M.; Shang, L.; Sheng, G.; Zhang, X.; Wen, X.; Wu, L.; Tung, C.; Zhang, T. Alumina-Supported CoFe Alloy Catalysts Derived from Layered-Double-Hydroxide Nanosheets for Efficient Photothermal CO<sub>2</sub> Hydrogenation to Hydrocarbons. *Adv. Mater.* **2018**, *30* (3), 1704663.

(48) O'Brien, P. G.; Ghuman, K. K.; Jelle, A. A.; Sandhel, A.; Wood, T. E.; Loh, J. Y. Y.; Jia, J.; Perovic, D.; Singh, C. V.; Kherani, N. P.; Mims, C. A.; Ozin, G. A. Enhanced Photothermal Reduction of Gaseous CO<sub>2</sub> over Silicon Photonic Crystal Supported Ruthenium at Ambient Temperature. *Energy Environ. Sci.* **2018**, *11* (12), 3443–3451.

(49) Wu, D.; Deng, K.; Hu, B.; Lu, Q.; Liu, G.; Hong, X. Plasmon-Assisted Photothermal Catalysis of Low-Pressure CO<sub>2</sub> Hydrogenation to Methanol over Pd/ZnO Catalyst. *ChemCatChem* **2019**, *11* (6), 1598–1601.

(50) Ren, J.; Ouyang, S.; Xu, H.; Meng, X.; Wang, T.; Wang, D.; Ye, J. Targeting Activation of CO<sub>2</sub> and H<sub>2</sub> over Ru-Loaded Ultrathin Layered Double Hydroxides to Achieve Efficient Photothermal CO<sub>2</sub> Methanation in Flow-Type System. *Adv. Energy Mater.* **2017**, *7* (5), 1601657.

(51) Guzman, M. S.; Rengasamy, K.; Binkley, M. M.; Jones, C.; Ranaivoarisoa, T. O.; Singh, R.; Fike, D. A.; Meacham, J. M.; Bose, A. Phototrophic Extracellular Electron Uptake Is Linked to Carbon Dioxide Fixation in the Bacterium *Rhodospseudomonas Palustris*. *Nat. Commun.* **2019**, *10* (1), 1355.

(52) Woo, H. M. Solar-to-Chemical and Solar-to-Fuel Production from CO<sub>2</sub> by Metabolically Engineered Microorganisms. *Curr. Opin. Biotechnol.* **2017**, *45*, 1–7.

(53) Liu, C.; Gallagher, J. J.; Sakimoto, K. K.; Nichols, E. M.; Chang, C. J.; Chang, M. C. Y.; Yang, P. Nanowire-Bacteria Hybrids for Unassisted Solar Carbon Dioxide Fixation to Value-Added Chemicals. *Nano Lett.* **2015**, *15* (5), 3634–3639.

(54) Osterloh, F. E. Photocatalysis versus Photosynthesis: A Sensitivity Analysis of Devices for Solar Energy Conversion and Chemical Transformations. *ACS Energy Lett.* **2017**, *2* (2), 445–453.

(55) Rajeshwar, K.; Thomas, A.; Janaky, C. Photocatalytic Activity of Inorganic Semiconductor Surfaces: Myths, Hype, and Reality. *J. Phys. Chem. Lett.* **2015**, *6* (1), 139–147.

(56) Xiao, M.; Wang, Z.; Luo, B.; Wang, S.; Wang, L. Enhancing Photocatalytic Activity of Tantalum Nitride by Rational Suppression of Bulk, Interface and Surface Charge Recombination. *Appl. Catal., B* **2019**, *246*, 195–201.

(57) Kamat, P. V.; Jin, S. Semiconductor Photocatalysis: “Tell Us the Complete Story! *ACS Energy Lett.* **2018**, *3* (3), 622–623.

(58) Kramm, U. I.; Marschall, R.; Rose, M. Pitfalls in Heterogeneous Thermal, Electro- and Photocatalysis. *ChemCatChem* **2019**, *11* (11), 2563–2574.

(59) Chang, X.; Wang, T.; Yang, P.; Zhang, G.; Gong, J. The Development of Cocatalysts for Photoelectrochemical CO<sub>2</sub> Reduction. *Adv. Mater.* **2019**, *31* (31), 1804710.

(60) Song, J. T.; Ryoo, H.; Cho, M.; Kim, J.; Kim, J. G.; Chung, S.-Y.; Oh, J. Nanoporous Au Thin Films on Si Photoelectrodes for Selective and Efficient Photoelectrochemical CO<sub>2</sub> Reduction. *Adv. Energy Mater.* **2017**, *7* (3), 1601103.

(61) Pastor, E.; Le Formal, F.; Mayer, M. T.; Tilley, S. D.; Francàs, L.; Mesa, C. A.; Grätzel, M.; Durrant, J. R. Spectroelectrochemical Analysis of the Mechanism of (Photo)Electrochemical Hydrogen Evolution at a Catalytic Interface. *Nat. Commun.* **2017**, *8* (1), 14280.

(62) Zhang, D.; Shi, J.; Zi, W.; Wang, P.; Liu, S. F. Recent Advances in Photoelectrochemical Applications of Silicon Materials for Solar-to-Chemicals Conversion. *ChemSusChem* **2017**, *10* (22), 4324–4341.

(63) Rongé, J.; Bosserez, T.; Martel, D.; Nervi, C.; Boarino, L.; Taulelle, F.; Decher, G.; Bordiga, S.; Martens, J. A. Monolithic Cells for Solar Fuels. *Chem. Soc. Rev.* **2014**, *43* (23), 7963–7981.

(64) Nayak, P. K.; Mahesh, S.; Snaith, H. J.; Cahen, D. Photovoltaic Solar Cell Technologies: Analysing the State of the Art. *Nat. Rev. Mater.* **2019**, *4* (4), 269–285.

(65) Green, M. A.; Dunlop, E. D.; Hohl-Ebinger, J.; Yoshita, M.; Kopidakis, N.; Ho-Baillie, A. W. Y. Solar Cell Efficiency Tables (Version 55). *Prog. Photovoltaics* **2020**, *28* (1), 3–15.

(66) Best Research-Cell Efficiency Chart | Photovoltaic Research. <https://www.nrel.gov/pv/cell-efficiency.html> (accessed 2020-03-19).

(67) Liu, Z.; Sofia, S. E.; Laine, H. S.; Woodhouse, M.; Wieghold, S.; Peters, I. M.; Buonassisi, T. Revisiting Thin Silicon for Photovoltaics: A Technoeconomic Perspective. *Energy Environ. Sci.* **2020**, *13* (1), 12–23.

(68) Endrődi, B.; Bencsik, G.; Darvas, F.; Jones, R.; Rajeshwar, K.; Janáky, C. Continuous-Flow Electroreduction of Carbon Dioxide. *Prog. Energy Combust. Sci.* **2017**, *62*, 133–154.

(69) Kumaravel, V.; Bartlett, J.; Pillai, S. C. Photoelectrochemical Conversion of Carbon Dioxide (CO<sub>2</sub>) into Fuels and Value-Added Products. *ACS Energy Lett.* **2020**, *5* (2), 486–519.

(70) Akhundi, A.; Habibi-Yangjeh, A.; Abitorabi, M.; Rahim Pouran, S. Review on Photocatalytic Conversion of Carbon Dioxide to Value-Added Compounds and Renewable Fuels by Graphitic Carbon Nitride-Based Photocatalysts. *Catal. Rev.: Sci. Eng.* **2019**, *61* (4), 595–628.

(71) Hiragond, C.; Ali, S.; Sorcar, S.; In, S.-I. In Hierarchical Nanostructured Photocatalysts for CO<sub>2</sub> Photoreduction. *Catalysts* **2019**, *9* (4), 370.

(72) Christoforidis, K. C.; Fornasiero, P. Photocatalysis for Hydrogen Production and CO<sub>2</sub> Reduction: The Case of Copper-Catalysts. *ChemCatChem* **2019**, *11* (1), 368–382.

(73) Tjandra, A. D.; Huang, J. Photocatalytic Carbon Dioxide Reduction by Photocatalyst Innovation. *Chin. Chem. Lett.* **2018**, *29* (6), 734–746.

(74) Ma, Y.; Wang, Z.; Xu, X.; Wang, J. Review on Porous Nanomaterials for Adsorption and Photocatalytic Conversion of CO<sub>2</sub>. *Chin. J. Catal.* **2017**, *38* (12), 1956–1969.

(75) Huang, Z.; Teramura, K.; Asakura, H.; Hosokawa, S.; Tanaka, T. Recent Progress in Photocatalytic Conversion of Carbon Dioxide



over Gallium Oxide and Its Nanocomposites. *Curr. Opin. Chem. Eng.* **2018**, *20*, 114–121.

(76) Sun, H.; Wang, S. Research Advances in the Synthesis of Nanocarbon-Based Photocatalysts and Their Applications for Photocatalytic Conversion of Carbon Dioxide to Hydrocarbon Fuels. *Energy Fuels* **2014**, *28* (1), 22–36.

(77) Low, J.; Cheng, B.; Yu, J.; Jaroniec, M. Carbon-Based Two-Dimensional Layered Materials for Photocatalytic CO<sub>2</sub> Reduction to Solar Fuels. *Energy Storage Mater.* **2016**, *3*, 24–35.

(78) Chen, X.; Jin, F. Photocatalytic Reduction of Carbon Dioxide by Titanium Oxide-Based Semiconductors to Produce Fuels. *Front. Energy* **2019**, *13* (2), 207–220.

(79) Abdullah, H.; Khan, M. M. R.; Ong, H. R.; Yaakob, Z. Modified TiO<sub>2</sub> Photocatalyst for CO<sub>2</sub> Photocatalytic Reduction: An Overview. *J. CO<sub>2</sub> Util.* **2017**, *22*, 15–32.

(80) Shehzad, N.; Tahir, M.; Johari, K.; Murugesan, T.; Hussain, M. A Critical Review on TiO<sub>2</sub> Based Photocatalytic CO<sub>2</sub> Reduction System: Strategies to Improve Efficiency. *J. CO<sub>2</sub> Util.* **2018**, *26*, 98–122.

(81) Xie, H.; Wang, J.; Ithisuphalap, K.; Wu, G.; Li, Q. Recent Advances in Cu-Based Nanocomposite Photocatalysts for CO<sub>2</sub> Conversion to Solar Fuels. *J. Energy Chem.* **2017**, *26* (6), 1039–1049.

(82) Xiong, Z.; Lei, Z.; Li, Y.; Dong, L.; Zhao, Y.; Zhang, J. A Review on Modification of Facet-Engineered TiO<sub>2</sub> for Photocatalytic CO<sub>2</sub> Reduction. *J. Photochem. Photobiol., C* **2018**, *36*, 24–47.

(83) Chen, D.; Zhang, X.; Lee, A. F. Synthetic Strategies to Nanostructured Photocatalysts for CO<sub>2</sub> Reduction to Solar Fuels and Chemicals. *J. Mater. Chem. A* **2015**, *3* (28), 14487–14516.

(84) Razzaq, A.; In, S. TiO<sub>2</sub> Based Nanostructures for Photocatalytic CO<sub>2</sub> Conversion to Valuable Chemicals. *Micromachines* **2019**, *10* (5), 326.

(85) Yang, M. Q.; Xu, Y. J. Photocatalytic Conversion of CO<sub>2</sub> over Graphene-Based Composites: Current Status and Future Perspective. *Nanoscale Horiz.* **2016**, *1* (3), 185–200.

(86) Shen, M.; Zhang, L.; Shi, J. Converting CO<sub>2</sub> into Fuels by Graphitic Carbon Nitride-Based Photocatalysts. *Nanotechnology* **2018**, *29*, 412001.

(87) Zeng, S.; Kar, P.; Thakur, U. K.; Shankar, K. A Review on Photocatalytic CO<sub>2</sub> Reduction Using Perovskite Oxide Nanomaterials. *Nanotechnology* **2018**, *29*, 052001.

(88) Voiry, D.; Shin, H. S.; Loh, K. P.; Chhowalla, M. Low-Dimensional Catalysts for Hydrogen Evolution and CO<sub>2</sub> Reduction. *Nat. Rev. Chem.* **2018**, *2* (1), 105.

(89) Li, X.; Wen, J.; Low, J.; Fang, Y.; Yu, J. Design and Fabrication of Semiconductor Photocatalyst for Photocatalytic Reduction of CO<sub>2</sub> to Solar Fuel. *Sci. China Mater.* **2014**, *57* (1), 70–100.

(90) Shi, R.; Waterhouse, G. I. N.; Zhang, T. Recent Progress in Photocatalytic CO<sub>2</sub> Reduction Over Perovskite Oxides. *Sol. RRL* **2017**, *1* (11), 1700126.

(91) Low, J.; Cheng, B.; Yu, J. Surface Modification and Enhanced Photocatalytic CO<sub>2</sub> Reduction Performance of TiO<sub>2</sub>: A Review. *Appl. Surf. Sci.* **2017**, *392*, 658–686.

(92) Ola, O.; Maroto-Valer, M. M. Review of Material Design and Reactor Engineering on TiO<sub>2</sub> Photocatalysis for CO<sub>2</sub> Reduction. *J. Photochem. Photobiol., C* **2015**, *24*, 16–42.

(93) Das, S.; Wan Daud, W. M. A. Photocatalytic CO<sub>2</sub> Transformation into Fuel: A Review on Advances in Photocatalyst and Photoreactor. *Renewable Sustainable Energy Rev.* **2014**, *39*, 765–805.

(94) Kumar, S.; Jain, S.; Yadav Lamba, B.; Kumar, P. Epigrammatic Status and Perspective of Sequestration of Carbon Dioxide: Role of TiO<sub>2</sub> as Photocatalyst. *Sol. Energy* **2018**, *159*, 423–433.

(95) Ali, S.; Flores, M. C.; Razzaq, A.; Sorcar, S.; Hiragond, C. B.; Kim, H. R.; Park, Y. H.; Hwang, Y.; Kim, H. S.; Kim, H.; Gong, E. H.; Lee, J.; Kim, D.; In, S. Gas Phase Photocatalytic CO<sub>2</sub> Reduction, “A Brief Overview for Benchmarking. *Catalysts* **2019**, *9* (9), 727.

(96) Roy, N.; Suzuki, N.; Terashima, C.; Fujishima, A. Recent Improvements in the Production of Solar Fuels: From CO<sub>2</sub> Reduction to Water Splitting and Artificial Photosynthesis. *Bull. Chem. Soc. Jpn.* **2019**, *92* (1), 178–192.

(97) Neațu, Ș.; Maciá-Agulló, J. A.; Garcia, H. Solar Light Photocatalytic CO<sub>2</sub> Reduction: General Considerations and Selected Bench-Mark Photocatalysts. *Int. J. Mol. Sci.* **2014**, *15* (4), 5246–5262.

(98) Ganesh, I. Conversion of Carbon Dioxide into Methanol - A Potential Liquid Fuel: Fundamental Challenges and Opportunities (a Review). *Renewable Sustainable Energy Rev.* **2014**, *31*, 221–257.

(99) Choi, J. Y.; Lim, C. K.; Park, B.; Kim, M.; Jamal, A.; Song, H. Surface Activation of Cobalt Oxide Nanoparticles for Photocatalytic Carbon Dioxide Reduction to Methane. *J. Mater. Chem. A* **2019**, *7* (25), 15068–15072.

(100) Li, X.; Sun, Y.; Xu, J.; Shao, Y.; Wu, J.; Xu, X.; Pan, Y.; Ju, H.; Zhu, J.; Xie, Y. Selective Visible-Light-Driven Photocatalytic CO<sub>2</sub> Reduction to CH<sub>4</sub> Mediated by Atomically Thin CuIn<sub>5</sub>S<sub>8</sub> Layers. *Nat. Energy* **2019**, *4* (8), 690–699.

(101) Pang, R.; Teramura, K.; Asakura, H.; Hosokawa, S.; Tanaka, T. Effect of Thickness of Chromium Hydroxide Layer on Ag Cocatalyst Surface for Highly Selective Photocatalytic Conversion of CO<sub>2</sub> by H<sub>2</sub>O. *ACS Sustainable Chem. Eng.* **2019**, *7* (2), 2083–2090.

(102) Xu, Y.; Mo, J.; Fu, Z. C.; Liu, S.; Yang, Z.; Fu, W. F. An Exceptionally Efficient Co-Co<sub>2</sub>P@N, P-Codoped Carbon Hybrid Catalyst for Visible Light-Driven CO<sub>2</sub>-to-CO Conversion. *Chem. - Eur. J.* **2018**, *24* (34), 8596–8602.

(103) Kuriki, R.; Sekizawa, K.; Ishitani, O.; Maeda, K. Visible-Light-Driven CO<sub>2</sub> Reduction with Carbon Nitride: Enhancing the Activity of Ruthenium Catalysts. *Angew. Chem., Int. Ed.* **2015**, *54* (8), 2406–2409.

(104) Genoni, A.; Chiridon, D. N.; Boniolo, M.; Sartorel, A.; Bernhard, S.; Bonchio, M. Tuning Iridium Photocatalysts and Light Irradiation for Enhanced CO<sub>2</sub> Reduction. *ACS Catal.* **2017**, *7* (1), 154–160.

(105) Yang, H.; Han, N.; Deng, J.; Wu, J.; Wang, Y.; Hu, Y.; Ding, P.; Li, Y.; Li, Y.; Lu, J. Selective CO<sub>2</sub> Reduction on 2D Mesoporous Bi Nanosheets. *Adv. Energy Mater.* **2018**, *8* (35), 1801536.

(106) Chen, J.; Yin, J.; Zheng, X.; Ait Ahsaine, H.; Zhou, Y.; Dong, C.; Mohammed, O. F.; Takanabe, K.; Bakr, O. M. Compositionally Screened Eutectic Catalytic Coatings on Halide Perovskite Photocathodes for Photoassisted Selective CO<sub>2</sub> Reduction. *ACS Energy Lett.* **2019**, *4* (6), 1279–1286.

(107) Schreier, M.; Gao, P.; Mayer, M. T.; Luo, J.; Moehl, T.; Nazeeruddin, M. K.; Tilley, S. D.; Grätzel, M. Efficient and Selective Carbon Dioxide Reduction on Low Cost Protected Cu<sub>2</sub>O Photocathodes Using a Molecular Catalyst. *Energy Environ. Sci.* **2015**, *8* (3), 855–861.

(108) Yuan, J.; Yang, L.; Hao, C. Communication—Lithium-Doped CuFeO<sub>2</sub> Thin Film Electrodes for Photoelectrochemical Reduction of Carbon Dioxide to Methanol. *J. Electrochem. Soc.* **2019**, *166* (14), H718–H720.

(109) Kang, U.; Choi, S. K.; Ham, D. J.; Ji, S. M.; Choi, W.; Han, D. S.; Abdel-Wahab, A.; Park, H. Photosynthesis of Formate from CO<sub>2</sub> and Water at 1% Energy Efficiency via Copper Iron Oxide Catalysis. *Energy Environ. Sci.* **2015**, *8* (9), 2638–2643.

(110) Kang, U.; Yoon, S. H.; Han, D. S.; Park, H. Synthesis of Aliphatic Acids from CO<sub>2</sub> and Water at Efficiencies Close to the Photosynthesis Limit Using Mixed Copper and Iron Oxide Films. *ACS Energy Lett.* **2019**, *4* (9), 2075–2080.

(111) Schreier, M.; Héroguel, F.; Steier, L.; Ahmad, S.; Luterbacher, J. S.; Mayer, M. T.; Luo, J.; Grätzel, M. Solar Conversion of CO<sub>2</sub> to CO Using Earth-Abundant Electrocatalysts Prepared by Atomic Layer Modification of CuO. *Nat. Energy* **2017**, *2* (7), 17087.

(112) Zhou, L. Q.; Ling, C.; Zhou, H.; Wang, X.; Liao, J.; Reddy, G. K.; Deng, L.; Peck, T. C.; Zhang, R.; Whittingham, M. S.; Wang, C.; Chu, C.; Yao, Y.; Jia, H. A High-Performance Oxygen Evolution Catalyst in Neutral-pH for Sunlight-Driven CO<sub>2</sub> Reduction. *Nat. Commun.* **2019**, *10* (1), 4081.

(113) Wang, Y.; Liu, J.; Wang, Y.; Wang, Y.; Zheng, G. Efficient Solar-Driven Electrocatalytic CO<sub>2</sub> Reduction in a Redox-Medium-Assisted System. *Nat. Commun.* **2018**, *9* (1), 5003.

(114) Cheng, W.; Richter, M. H.; Sullivan, I.; Larson, D. M.; Xiang, C.; Brunschwigg, B. S.; Atwater, H. A.; Xiang, C.; Brunschwigg, B. S.;

Atwater, H. A. CO<sub>2</sub> Reduction to CO with 19% Efficiency in a Solar-Driven Gas Diffusion Electrode Flow Cell under Outdoor Solar Illumination. *ACS Energy Lett.* **2020**, *5* (2), 470–476.

(115) Ma, M.; Liu, K.; Shen, J.; Kas, R.; Smith, W. A. In Situ Fabrication and Reactivation of Highly Selective and Stable Ag Catalysts for Electrochemical CO<sub>2</sub> Conversion. *ACS Energy Lett.* **2018**, *3* (6), 1301–1306.

(116) Zhao, S.; Jin, R.; Jin, R. Opportunities and Challenges in CO<sub>2</sub> Reduction by Gold- and Silver-Based Electrocatalysts: From Bulk Metals to Nanoparticles and Atomically Precise Nanoclusters. *ACS Energy Lett.* **2018**, *3* (2), 452–462.

(117) Kodaimati, M. S.; McClelland, K. P.; He, C.; Lian, S.; Jiang, Y.; Zhang, Z.; Weiss, E. A. Viewpoint: Challenges in Colloidal Photocatalysis and Some Strategies for Addressing Them. *Inorg. Chem.* **2018**, *57* (7), 3659–3670.

(118) Wang, K.; Lu, H.; Zhu, X.; Lin, Y.; Beard, M. C.; Yan, Y.; Chen, X. Ultrafast Reaction Mechanisms in Perovskite Based Photocatalytic C–C Coupling. *ACS Energy Lett.* **2020**, *5* (2), 566–571.

(119) Samu, G. F.; Balog, A.; De Angelis, F.; Meggiolaro, D.; Kamat, P. V.; Janáky, C. Electrochemical Hole Injection Selectively Expels Iodide from Mixed Halide Perovskite Films. *J. Am. Chem. Soc.* **2019**, *141* (27), 10812–10820.

(120) Beranek, R. Selectivity of Chemical Conversions: Do Light-Driven Photoelectrocatalytic Processes Hold Special Promise? *Angew. Chem., Int. Ed.* **2019**, *58* (47), 16724–16729.

(121) Li, H.; Zhang, X.; MacFarlane, D. R. Carbon Quantum Dots/Cu<sub>2</sub>O Heterostructures for Solar-Light-Driven Conversion of CO<sub>2</sub> to Methanol. *Adv. Energy Mater.* **2015**, *5* (5), 1401077.

(122) Brito, J. F.; Genovese, C.; Tavella, F.; Ampelli, C.; Boldrin Zanoni, M. V.; Centi, G.; Perathoner, S. CO<sub>2</sub> Reduction of Hybrid Cu<sub>2</sub>O–Cu/Gas Diffusion Layer Electrodes and Their Integration in a Cu-based Photoelectrocatalytic Cell. *ChemSusChem* **2019**, *12* (18), 4274–4284.

(123) Kim, J. H.; Magesh, G.; Kang, H. J.; Banu, M.; Kim, J. H.; Lee, J.; Lee, J. S. Carbonate-Coordinated Cobalt Co-Catalyzed BiVO<sub>4</sub>/WO<sub>3</sub> Composite Photoanode Tailored for CO<sub>2</sub> Reduction to Fuels. *Nano Energy* **2015**, *15*, 153–163.

(124) Chang, X.; Wang, T.; Zhao, Z. J.; Yang, P.; Greeley, J.; Mu, R.; Zhang, G.; Gong, Z.; Luo, Z.; Chen, J.; Cui, Y.; Ozin, G. A.; Gong, J. Tuning Cu/Cu<sub>2</sub>O Interfaces for the Reduction of Carbon Dioxide to Methanol in Aqueous Solutions. *Angew. Chem., Int. Ed.* **2018**, *57* (47), 15415–15419.

(125) Huan, T. N.; Dalla Corte, D. A.; Lamaison, S.; Karapinar, D.; Lutz, L.; Menguy, N.; Foldyna, M.; Turren-Cruz, S. H.; Hagfeldt, A.; Bella, F.; Fontecave, M.; Mougél, V. Low-Cost High-Efficiency System for Solar-Driven Conversion of CO<sub>2</sub> to Hydrocarbons. *Proc. Natl. Acad. Sci. U. S. A.* **2019**, *116* (20), 9735–9740.

(126) Deb Nath, N. C.; Choi, S. Y.; Jeong, H. W.; Lee, J. J.; Park, H. Stand-Alone Photoconversion of Carbon Dioxide on Copper Oxide Wire Arrays Powered by Tungsten Trioxide/Dye-Sensitized Solar Cell Dual Absorbers. *Nano Energy* **2016**, *25*, 51–59.

(127) Yu, S.; Jain, P. K. Plasmonic Photosynthesis of C<sub>1</sub>–C<sub>3</sub> Hydrocarbons from Carbon Dioxide Assisted by an Ionic Liquid. *Nat. Commun.* **2019**, *10* (1), 2022.

(128) Sagara, N.; Kamimura, S.; Tsubota, T.; Ohno, T. Photoelectrochemical CO<sub>2</sub> Reduction by a P-Type Boron-Doped g-C<sub>3</sub>N<sub>4</sub> Electrode under Visible Light. *Appl. Catal., B* **2016**, *192*, 193–198.

(129) Mateo, D.; Asiri, A. M.; Albergo, J.; García, H. The Mechanism of Photocatalytic CO<sub>2</sub> Reduction by Graphene-Supported Cu<sub>2</sub>O Probed by Sacrificial Electron Donors. *Photochem. Photobiol. Sci.* **2018**, *17* (6), 829–834.

(130) Ci, C.; Carbó, J. J.; Neumann, R.; Graaf, C. De; Poblet, J. M. Photoreduction Mechanism of CO<sub>2</sub> to CO Catalyzed by a Rhenium(I)-Polyoxometalate Hybrid Compound. *ACS Catal.* **2016**, *6* (10), 6422–6428.

(131) Zheng, Y.; Zhang, W.; Li, Y.; Chen, J.; Yu, B.; Wang, J.; Zhang, L.; Zhang, J. Energy Related CO<sub>2</sub> Conversion and Utilization: Advanced Materials/Nanomaterials, Reaction Mechanisms and Technologies. *Nano Energy* **2017**, *40*, 512–539.

(132) Poudyal, S.; Laursen, S. Photocatalytic CO<sub>2</sub> Reduction by H<sub>2</sub>O: Insights from Modeling Electronically Relaxed Mechanisms. *Catal. Sci. Technol.* **2019**, *9* (4), 1048–1059.

(133) Karamian, E.; Sharifnia, S. On the General Mechanism of Photocatalytic Reduction of CO<sub>2</sub>. *J. CO<sub>2</sub> Util.* **2016**, *16*, 194–203.

(134) Kang, H. Y.; Nam, D. H.; Yang, K. D.; Joo, W.; Kwak, H.; Kim, H. H.; Hong, S. H.; Nam, K. T.; Joo, Y. C. Synthetic Mechanism Discovery of Monophase Cuprous Oxide for Record High Photoelectrochemical Conversion of CO<sub>2</sub> to Methanol in Water. *ACS Nano* **2018**, *12* (8), 8187–8196.

(135) Uzunova, E. L.; Seriani, N.; Mikosch, H. CO<sub>2</sub> Conversion to Methanol on Cu(I) Oxide Nanolayers and Clusters: An Electronic Structure Insight into the Reaction Mechanism. *Phys. Chem. Chem. Phys.* **2015**, *17* (16), 11088–11094.

(136) Yin, G.; Huang, X.; Chen, T.; Zhao, W.; Bi, Q.; Xu, J.; Han, Y.; Huang, F. Hydrogenated Blue Titania for Efficient Solar to Chemical Conversions: Preparation, Characterization, and Reaction Mechanism of CO<sub>2</sub> Reduction. *ACS Catal.* **2018**, *8* (2), 1009–1017.

(137) Meister, S.; Reithmeier, R. O.; Tschurl, M.; Heiz, U.; Rieger, B. Unraveling Side Reactions in the Photocatalytic Reduction of CO<sub>2</sub>: Evidence for Light-Induced Deactivation Processes in Homogeneous Photocatalysis. *ChemCatChem* **2015**, *7* (4), 690–697.

(138) Sommers, J. M.; Alderman, N. P.; Viasus, C. J.; Gambarotta, S. Revisiting the Behaviour of BiVO<sub>4</sub> as a Carbon Dioxide Reduction Photo-Catalyst. *Dalt. Trans.* **2017**, *46* (19), 6404–6408.

(139) Sriramagiri, G. M.; Ahmed, N.; Luc, W.; Dobson, K. D.; Hegedus, S. S.; Jiao, F. Toward a Practical Solar-Driven CO<sub>2</sub> Flow Cell Electrolyzer: Design and Optimization. *ACS Sustainable Chem. Eng.* **2017**, *5* (11), 10959–10966.

(140) Endrődi, B.; Kecsenovity, E.; Samu, A.; Darvas, F.; Jones, R. V.; Török, V.; Danyi, A.; Janáky, C. Multilayer Electrolyzer Stack Converts Carbon Dioxide to Gas Products at High Pressure with High Efficiency. *ACS Energy Lett.* **2019**, *4* (7), 1770–1777.

(141) Urbain, F.; Tang, P.; Carretero, N. M.; Andreu, T.; Gerling, L. G.; Voz, C.; Arbiol, J.; Morante, J. R. A Prototype Reactor for Highly Selective Solar-Driven CO<sub>2</sub> Reduction to Synthesis Gas Using Nanosized Earth-Abundant Catalysts and Silicon Photovoltaics. *Energy Environ. Sci.* **2017**, *10* (10), 2256–2266.

(142) Haas, T.; Krause, R.; Weber, R.; Demler, M.; Schmid, G. Technical Photosynthesis Involving CO<sub>2</sub> Electrolysis and Fermentation. *Nat. Catal.* **2018**, *1* (1), 32–39.

(143) Ren, D.; Loo, N. W. X.; Gong, L.; Yeo, B. S. Continuous Production of Ethylene from Carbon Dioxide and Water Using Intermittent Sunlight. *ACS Sustainable Chem. Eng.* **2017**, *5* (10), 9191–9199.

(144) Deng, W.; Zhang, L.; Dong, H.; Chang, X.; Wang, T.; Gong, J. Achieving Convenient CO<sub>2</sub> Electrorreduction and Photovoltage in Tandem Using Potential-Insensitive Disordered Ag Nanoparticles. *Chem. Sci.* **2018**, *9* (32), 6599–6604.

(145) Kim, B. J.; Piao, G.; Kim, S.; Yang, S. Y.; Park, Y.; Han, D. S.; Shon, H. K.; Hoffmann, M. R.; Park, H. High-Efficiency Solar Desalination Accompanying Electrocatalytic Conversions of Desalted Chloride and Captured Carbon Dioxide. *ACS Sustainable Chem. Eng.* **2019**, *7* (18), 15320–15328.

(146) Gurudayal; Bullock, J.; Srankó, D. F.; Towle, C. M.; Lum, Y.; Hettick, M.; Scott, M. C.; Javey, A.; Ager, J. Efficient Solar-Driven Electrochemical CO<sub>2</sub> Reduction to Hydrocarbons and Oxygenates. *Energy Environ. Sci.* **2017**, *10* (10), 2222–2230.

(147) Wang, L.; Sofer, Z.; Pumera, M. Will Any Crap We Put into Graphene Increase Its Electrocatalytic Effect? *ACS Nano* **2020**, *14* (1), 21–25.

(148) Zhou, X.; Xiang, C. Comparative Analysis of Solar-to-Fuel Conversion Efficiency: A Direct, One-Step Electrochemical CO<sub>2</sub> Reduction Reactor versus a Two-Step, Cascade Electrochemical CO<sub>2</sub> Reduction Reactor. *ACS Energy Lett.* **2018**, *3* (8), 1892–1897.

(149) Higgins, D.; Hahn, C.; Xiang, C.; Jaramillo, T. F.; Weber, A. Z. Gas-Diffusion Electrodes for Carbon Dioxide Reduction: A New Paradigm. *ACS Energy Lett.* **2019**, *4* (1), 317–324.

- (150) Szczesny, J.; Ruff, A.; Oliveira, A. R.; Pita, M.; Pereira, I. A. C.; De Lacey, A. L.; Schuhmann, W. Electroenzymatic CO<sub>2</sub> Fixation Using Redox Polymer/Enzyme-Modified Gas Diffusion Electrodes. *ACS Energy Lett.* **2020**, *5*, 321–327.
- (151) Liu, K.; Smith, W. A.; Burdyny, T. Introductory Guide to Assembling and Operating Gas Diffusion Electrodes for Electrochemical CO<sub>2</sub> Reduction. *ACS Energy Lett.* **2019**, *4* (3), 639–643.
- (152) Liu, J.; Liu, B.; Ren, Y.; Yuan, Y.; Zhao, H.; Yang, H.; Liu, S. Hydrogenated Nanotubes/Nanowires Assembled from TiO<sub>2</sub> Nanoflakes with Exposed {111} Facets: Excellent Photo-Catalytic CO<sub>2</sub> Reduction Activity and Charge Separation Mechanism between (111) and (111) Polar Surfaces. *J. Mater. Chem. A* **2019**, *7* (24), 14761–14775.
- (153) Wan, L.; Zhou, Q.; Wang, X.; Wood, T. E.; Wang, L.; Duchesne, P. N.; Guo, J.; Yan, X.; Xia, M.; Li, Y. F.; Jelle, A. A.; Ulmer, U.; Jia, J.; Li, T.; Sun, W.; Ozin, G. A. Cu<sub>2</sub>O Nanocubes with Mixed Oxidation-State Facets for (Photo)Catalytic Hydrogenation of Carbon Dioxide. *Nat. Catal.* **2019**, *2* (10), 889–898.
- (154) Gao, C.; Meng, Q.; Zhao, K.; Yin, H.; Wang, D.; Guo, J.; Zhao, S.; Chang, L.; He, M.; Li, Q.; Zhao, H.; Huang, X.; Gao, Y.; Tang, Z. Co<sub>3</sub>O<sub>4</sub> Hexagonal Platelets with Controllable Facets Enabling Highly Efficient Visible-Light Photocatalytic Reduction of CO<sub>2</sub>. *Adv. Mater.* **2016**, *28* (30), 6485–6490.
- (155) Chen, Q.; Chen, X.; Fang, M.; Chen, J.; Li, Y.; Xie, Z.; Kuang, Q.; Zheng, L. Photo-Induced Au-Pd Alloying at TiO<sub>2</sub> {101} Facets Enables Robust CO<sub>2</sub> Photocatalytic Reduction into Hydrocarbon Fuels. *J. Mater. Chem. A* **2019**, *7* (3), 1334–1340.
- (156) Wu, Y. A.; McNulty, I.; Liu, C.; Lau, K. C.; Liu, Q.; Paulikas, A. P.; Sun, C. J.; Cai, Z.; Guest, J. R.; Ren, Y.; Stamenkovic, V.; Curtiss, L. A.; Liu, Y.; Rajh, T. Facet-Dependent Active Sites of a Single Cu<sub>2</sub>O Particle Photocatalyst for CO<sub>2</sub> Reduction to Methanol. *Nat. Energy* **2019**, *4* (11), 957–968.
- (157) Zhao, Y.; Wei, Y.; Wu, X.; Zheng, H.; Zhao, Z.; Liu, J.; Li, J. Graphene-Wrapped Pt/TiO<sub>2</sub> Photocatalysts with Enhanced Photo-generated Charges Separation and Reactant Adsorption for High Selective Photoreduction of CO<sub>2</sub> to CH<sub>4</sub>. *Appl. Catal., B* **2018**, *226*, 360–372.
- (158) Xia, C.; Zhu, P.; Jiang, Q.; Pan, Y.; Liang, W.; Stavitski, E.; Alshareef, H. N.; Wang, H. Continuous Production of Pure Liquid Fuel Solutions via Electrocatalytic CO<sub>2</sub> Reduction Using Solid-Electrolyte Devices. *Nat. Energy* **2019**, *4* (9), 776–785.
- (159) Kong, Z. C.; Liao, J. F.; Dong, Y. J.; Xu, Y. F.; Chen, H. Y.; Kuang, D.-B.; Su, C. Y. Core@shell CsPbBr<sub>3</sub>@zeolitic Imidazolate Framework Nanocomposite for Efficient Photocatalytic CO<sub>2</sub> Reduction. *ACS Energy Lett.* **2018**, *3* (11), 2656–2662.
- (160) Kecsenvity, E.; Endrödi, B.; Tóth, P. S.; Zou, Y.; Dryfe, R. A. W.; Rajeshwar, K.; Janáky, C. Enhanced Photoelectrochemical Performance of Cuprous Oxide/Graphene Nanohybrids. *J. Am. Chem. Soc.* **2017**, *139* (19), 6682–6692.
- (161) Kecsenvity, E.; Endrödi, B.; Pápa, Z.; Hernádi, K.; Rajeshwar, K.; Janáky, C. Decoration of Ultra-Long Carbon Nanotubes with Cu<sub>2</sub>O Nanocrystals: A Hybrid Platform for Enhanced Photoelectrochemical CO<sub>2</sub> Reduction. *J. Mater. Chem. A* **2016**, *4* (8), 3139–3147.
- (162) Kormányos, A.; Hursán, D.; Janáky, C. Photoelectrochemical Behavior of PEDOT/Nanocarbon Electrodes: Fundamentals and Structure-Property Relationships. *J. Phys. Chem. C* **2018**, *122* (25), 13682–13690.
- (163) Osterloh, F. E. Inorganic Nanostructures for Photoelectrochemical and Photocatalytic Water Splitting. *Chem. Soc. Rev.* **2013**, *42*, 2294–2320.
- (164) Rajeshwar, K. Electron Transfer at Semiconductor-Electrolyte Interfaces. *Electron Transfer in Chemistry*; Balzani, V., Ed.; Wiley-VCH: Weinheim, 2001.
- (165) Boettcher, S. W.; Spurgeon, J. M.; Putnam, M. C.; Warren, E. L.; Turner-Evans, D. B.; Kelzenberg, M. D.; Maiolo, J. R.; Atwater, H. A.; Lewis, N. S. Energy-Conversion Properties of Vapor-Liquid-Solid-Grown Silicon Wire-Array Photocathodes. *Science* **2010**, *327* (5962), 185–187.
- (166) Warren, E. L.; Atwater, H. A.; Lewis, N. S. Silicon Microwire Arrays for Solar Energy-Conversion Applications. *J. Phys. Chem. C* **2014**, *118* (2), 747–759.
- (167) Goodey, A. P.; Eichfeld, S. M.; Lew, K.-K.; Redwing, J. M.; Mallouk, T. E. Silicon Nanowire Array Photoelectrochemical Cells. *J. Am. Chem. Soc.* **2007**, *129* (41), 12344–12345.
- (168) Panayotov, D. A.; Frenkel, A. I.; Morris, J. R. Catalysis and Photocatalysis by Nanoscale Au/TiO<sub>2</sub>: Perspectives for Renewable Energy. *ACS Energy Lett.* **2017**, *2* (5), 1223–1231.
- (169) Negrín-Montecelo, Y.; Comesaña-Hermo, M.; Khorashad, L. K.; Sousa-Castillo, A.; Wang, Z.; Pérez-Lorenzo, M.; Liedl, T.; Govorov, A. O.; Correa-Duarte, M. A. Photophysical Effects behind the Efficiency of Hot Electron Injection in Plasmon-Assisted Catalysis: The Joint Role of Morphology and Composition. *ACS Energy Lett.* **2020**, *5* (2), 395–402.
- (170) Creel, E. B.; Corson, E. R.; Eichhorn, J.; Kostecki, R.; Urban, J. J.; McCloskey, B. D. Directing Selectivity of Electrochemical Carbon Dioxide Reduction Using Plasmonics. *ACS Energy Lett.* **2019**, *4* (5), 1098–1105.
- (171) Spitler, M. T.; Modestino, M. A.; Deutsch, T. G.; Xiang, C. X.; Durrant, J. R.; Esposito, D. V.; Haussener, S.; Maldonado, S.; Sharp, I. D.; Parkinson, B. A.; Ginley, D. S.; Houle, F. A.; Hannappel, T.; Neale, N. R.; Nocera, D. G.; McIntyre, P. C. Practical Challenges in the Development of Photoelectrochemical Solar Fuels Production. *Sustain. Energy Fuels* **2020**, *4* (3), 985–995.
- (172) Xu, P.; Huang, T.; Huang, J.; Yan, Y.; Mallouk, T. E. Dye-Sensitized Photoelectrochemical Water Oxidation through a Buried Junction. *Proc. Natl. Acad. Sci. U. S. A.* **2018**, *115* (27), 6946–6951.
- (173) Tembhumne, S.; Nandjou, F.; Haussener, S. A Thermally Synergistic Photo-Electrochemical Hydrogen Generator Operating under Concentrated Solar Irradiation. *Nat. Energy* **2019**, *4* (5), 399–407.
- (174) Verma, S.; Lu, S.; Kenis, P. J. A. Co-Electrolysis of CO<sub>2</sub> and Glycerol as a Pathway to Carbon Chemicals with Improved Technoeconomics Due to Low Electricity Consumption. *Nat. Energy* **2019**, *4* (6), 466–474.
- (175) Salvatore, D.; Berlinguette, C. P. Voltage Matters When Reducing CO<sub>2</sub> in an Electrochemical Flow Cell. *ACS Energy Lett.* **2020**, *5* (1), 215–220.
- (176) Castro, S.; Albo, J.; Irabien, A. Photoelectrochemical Reactors for CO<sub>2</sub> Utilization. *ACS Sustainable Chem. Eng.* **2018**, *6* (12), 15877–15894.